

# Appendix I

## Seismology

## **Analysis of Ground Motions from earthquakes at Cadia Mine, Australia**

*Sept. 10, 2018 – Draft Report V2*

*Gail M. Atkinson, Ph.D., P.Geo., FRSC*

---

### **Introduction**

This report presents an analysis of ground motions that were generated by the seismic events that occurred at the Cadia mine site from April 2017 through July 2018. There were five events of  $M \geq 3$  (where  $M$  is moment magnitude) during this time: an event of  $M 4.3$  on April 14, 2017; an event of  $M \sim 3.5$  on Nov 25, 2017, two events of  $M 3.0$  (10 seconds apart) on March 8, 2018, and an event of  $M \sim 3.1$  on July 22, 2018. The estimation of the moment magnitudes is described in the next section. The embankment failure at Cadia was noticed the day after the two events in March 2018. All five events produced ground motions strong enough to be felt nearby. The analysis considers regional seismographic data available from Geoscience Australia (through the IRIS data management centre at [www.iris.edu](http://www.iris.edu)), and on-site geophone and broadband seismometer recordings at the Cadia mine site, provided by IMS Seismology (by Aleksander Mendecki and Denver Birch, personal communication, April 2018, Aug. 2018).

The report focus is on: (i) the ground motions which occurred about a day before the failure (the March 8, 2018 events); and (ii) the strongest ground motions (those of April 2017). Motions from the Nov. 25, 2017 event would be intermediate in amplitude to the events of March 2018 and April 2017. On-site motions from the July 22, 2018 event were similar to those of March 8, though the July motions were larger at regional distances (hundreds of km). Ground motion analysis is used to construct time histories of motions that represent those that likely occurred at the failure location, as input at the bedrock level, resulting from the April 2017, March 2018, and July 2018 events. The time histories can be used as input (at the bedrock level) to explore the likely response of soils and structures at the failure site, including the possible cumulative effects of multiple events.

### **Seismic Setting and Ground Motion Recordings**

Figure 1 shows the overall seismicity setting of the Cadia Mine area based on the regional catalogue from Geoscience Australia (<https://earthquakes.ga.gov.au>). The regional network currently detects and locates only events of  $ML > \sim 2.5$  in the region, as the nearest stations are  $> 100$  km away; the regional networks are not capable of accurately locating events in the site area due to the sparse regional station distribution. From the regional catalogue, we observe that there is an apparent trend

of seismicity striking northwest-southeast through the Cadia site area. Most events are of small magnitude, with events of  $M > 3$  being concentrated near the Cadia site.

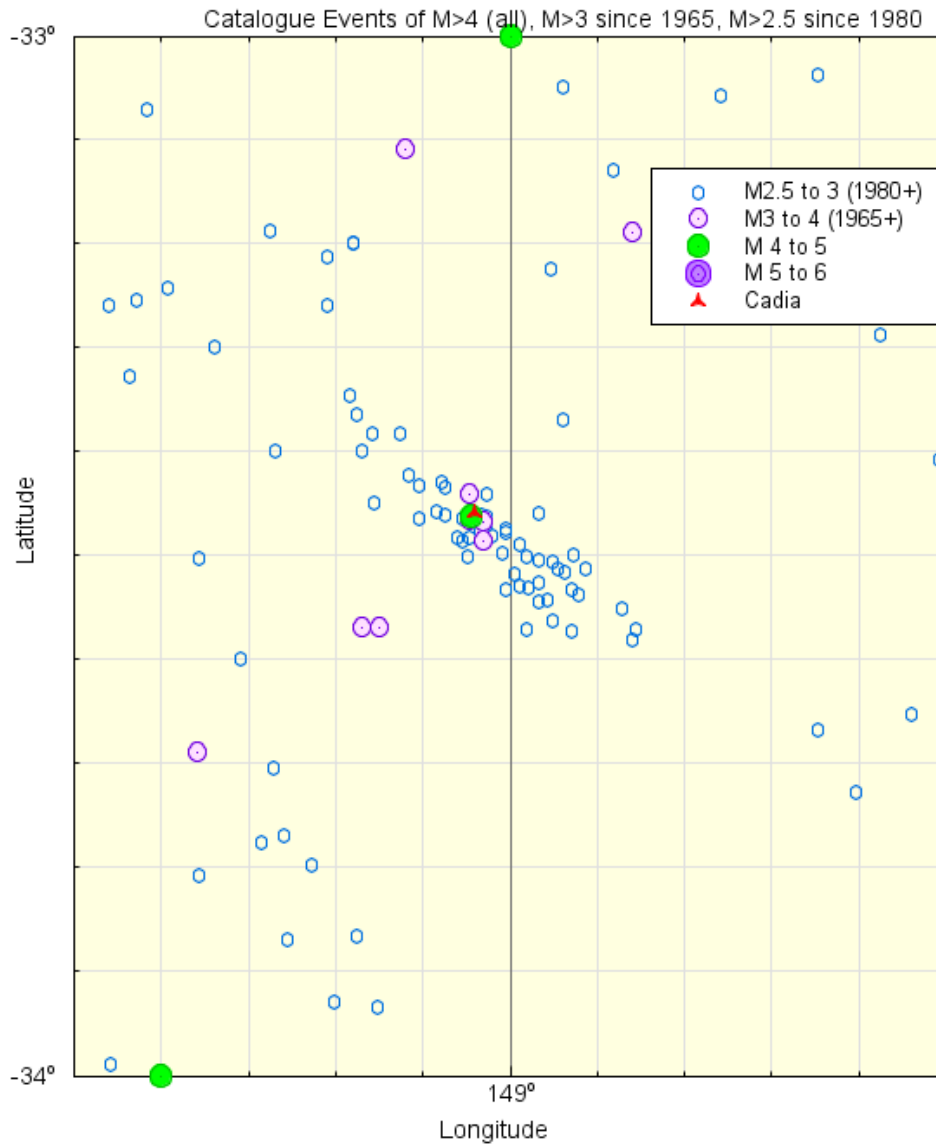


Figure 1 – Seismicity of Cadia region based on Geoscience Australia catalogue to May 31, 2018. The figure includes all known events of  $M \geq 4$  (where  $M$  is the catalogue magnitude, usually  $ML$ ), events of  $M \geq 3$  from 1965, and events of  $M \geq 2.5$  from 1980.

To obtain a more detailed look at the seismicity at Cadia, there is an extensive on-site array of geophones at the Cadia mine site, operated on behalf of Newcrest by IMS Seismology. The local network contains much more detailed information on the distribution of local events and provides much more accurate event locations. Figure

2 shows a representative distribution of local events at the mine site, using the accurate event locations as provided by IMS Seismology. Note that most of the events (including those of March 8) and monitoring sites are approximately 5 km away from the failure site.

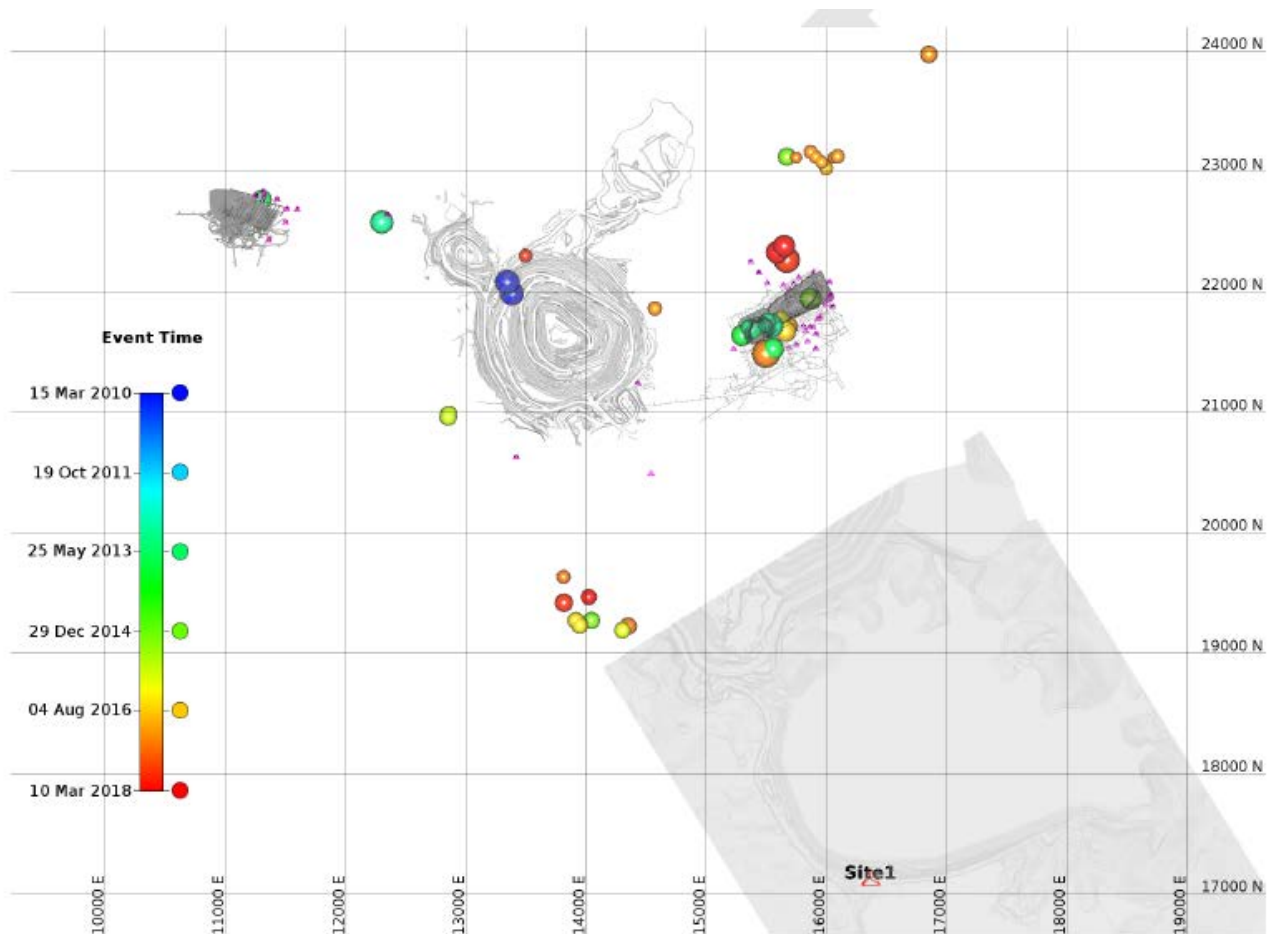


Figure 2 – Distribution of the larger seismic events in the Cadia site area (circles) to March 2018, in relation to monitoring sites (pink tetrahedra) and the March 9, 2018 failure site (Site 1). From IMS (2018).

Ground-motion data were analyzed in detail for the **M**4.3 2017 event, the **M**3.0 March 2018 and the **M**3.1 July 2018 event. The regional network stations are mostly broadband seismograph stations, whereas the local monitoring stations are geophones with natural frequencies of 4.5 Hz or 14 Hz. A broadband seismometer was installed by IMS in a temporary location near the failure site after the March 2018 events but before the July event. The waveform data from all regional broadband stations within 600 km were downloaded from IRIS and processed to obtain instrument-corrected response spectra (5% damped pseudo-spectral

acceleration, PSA). The processing includes windowing, digital filtering and removal of instrument response using the ICORRECT algorithm as described by Assatourians and Atkinson (2010). For the 2018 events, a single time window (several hundred seconds) captures both **M**3 events on the regional stations, because from the viewpoint of spectral response these two events are close enough in time to be considered as a single event. Response spectra for the local data for the March 2018 events were calculated by IMS (2018) (for selected records from each of the two events) and provided to the study. The recording conditions for the on-site geophone data are hard rock (>3000 m/s), and the local amplitudes provided by IMS represent the rms average of the 3 components (which tend to be similar for these mining sites, according to the IMS report). At regional distances, the recording conditions are unknown, and the horizontal and vertical components are considered. The horizontal components tend to be larger than the vertical, which is expected for all but very hard rock sites.

Figure 3 shows the response spectra amplitudes for the events to March 2018 in comparison to candidate ground-motion prediction equations (GMPEs) that express the expected scaling of motions with magnitude and distance. The additional data for the July 2018 event were analyzed subsequently and are described later. The candidate GMPEs are the Hassani and Atkinson (2018) generic model for hard rock sites, the Atkinson et al. (2015) model for rock sites in eastern North America, and the Atkinson (2015) model developed from events in California (soft-rock site conditions).

The Hassani and Atkinson (2018; HA18) model is particularly useful for this study because it allows for adjustment of both the selected stress parameter and the selected kappa value. Kappa is a site parameter that expressed the decay of high-frequency ground motion in the near-surface layers. Because the local recordings are at depth, on very hard rock conditions (>3000 m/s shear-wave velocity), a very low kappa applies (e.g. ~0.001), and there is essentially no attenuation of high-frequency motion due to site effects in the frequency range of interest. Based on this consideration and the fit to the observations (Figure 3), we select the HA18 model, with kappa=0.001, to represent the magnitude-distance scaling of motions. By inspection, the 2017 event is represented by **M**=4.3, and the 2018 events by **M**=3.0; these values of moment magnitude are consistent with the 1-Hz spectral amplitudes at both local and regional distances (see Atkinson et al., 2014). Both events have high frequency amplitudes (PSA at 10 Hz; see Novakovic et al., 2018) consistent with a stress parameter of 100 bars.

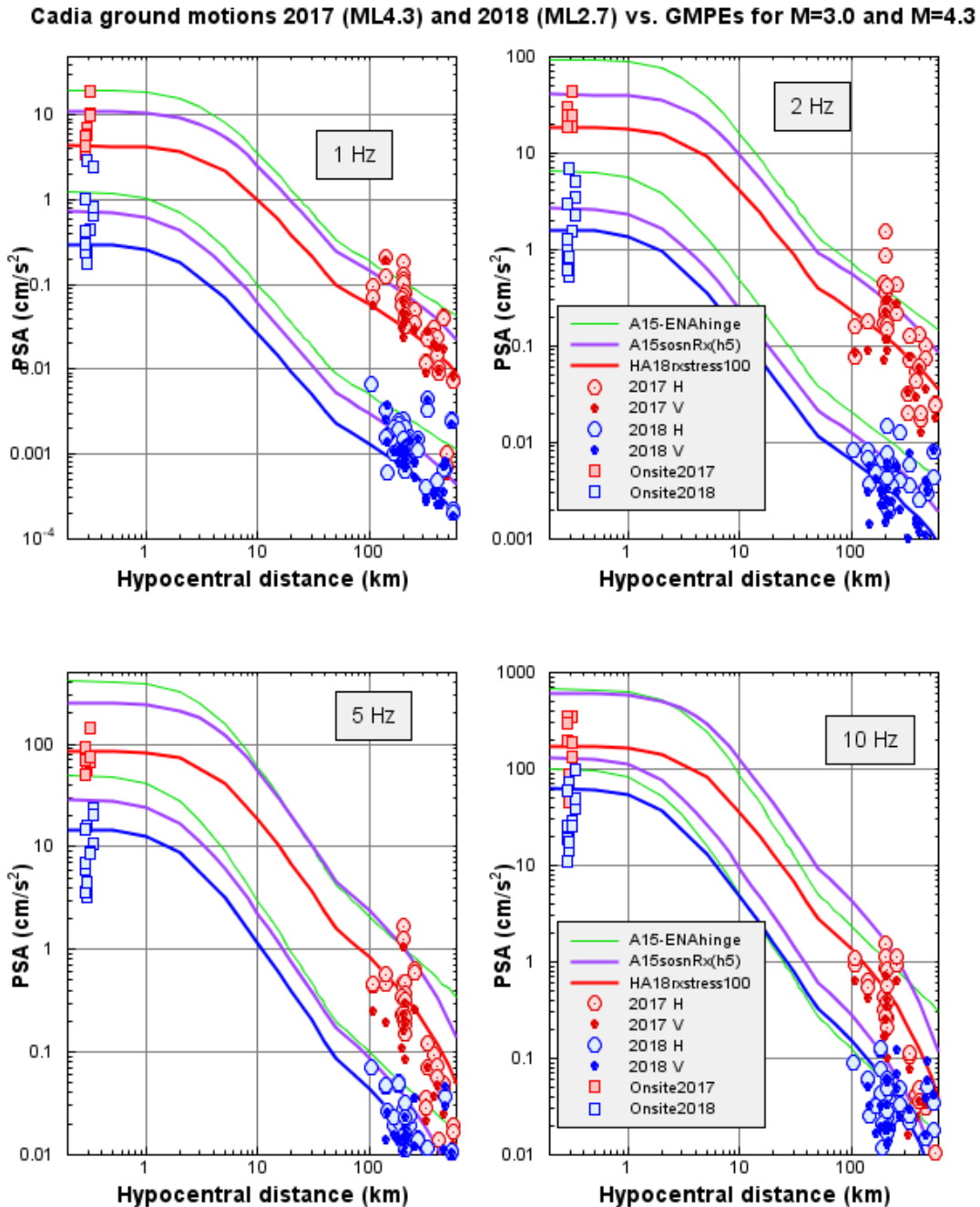


Figure 3 – Response spectral amplitudes ( $H$ =horizontal,  $V$ =vertical) for the 2017 (red) and 2018 (blue) events from onsite and regional broadband records, compared to GMPEs of Hassani and Atkinson (2018) for hard rock for  $M=3.0$  (blue) and 4.3 (red), stress = 100 bars. Purple and green lines show alternative GMPEs of Atkinson et al. (2015) for eastern North America (rock) and Atkinson (2015) for California (green), respectively.

## Development of Target Response Spectrum and Time Histories for Failure Site

Based on the good agreement of observed amplitudes and the HA18 GMPE for hard rock ( $\kappa=0.001$ , stress=100 bars) for  $M=3.0$  (2018) and  $M=4.3$  (2017) (Figure 3), we can use this model to define a target response spectrum for the location of the failure site, which is approximately 5 km from the earthquake source. To reflect amplitude variability, the target is defined as the median-plus-sigma amplitude, assuming a factor of two amplitude variability represents one standard deviation (sigma), at a hypocentral distance of 5 km. Accordingly, the motions at the failure site are assumed to follow the HA18 response spectrum (median\*2) for these conditions. Figure 4 shows this target spectrum for the two event scenarios. Note that this spectrum represents the input for hard rock conditions. We have good confidence in this spectrum because it has been calibrated with observations at both local and regional distances, as illustrated in Figure 3.

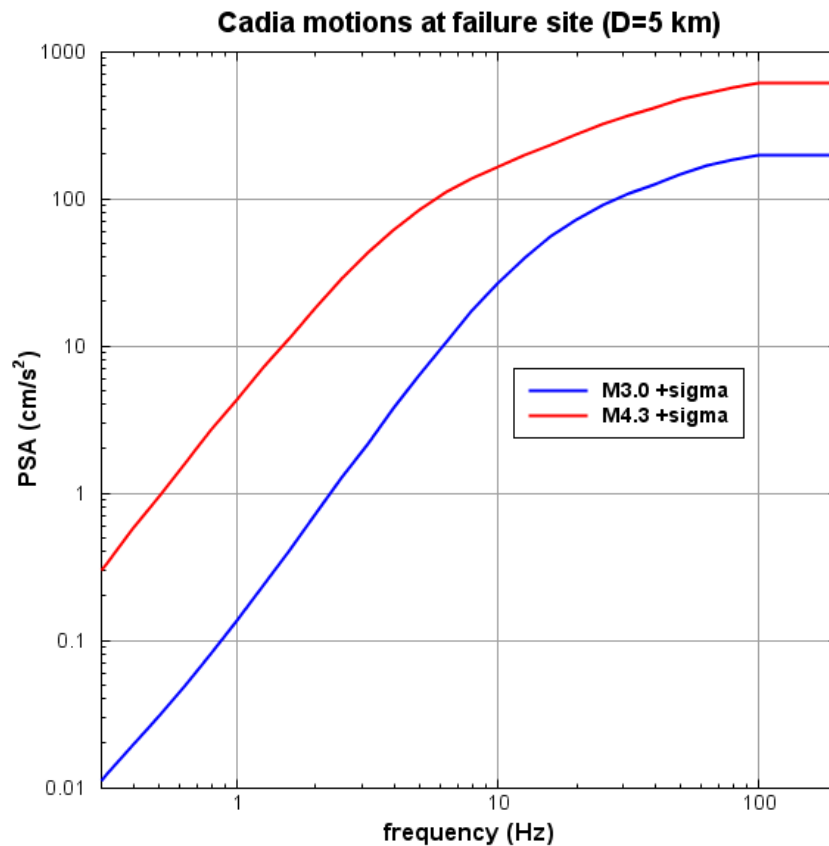


Figure 4 – Inferred spectrum at the failure site (~5 km from source) based on HA18 GMPE (median\*2) for  $M=3.0$  and  $M=4.3$  ( $\kappa=0.001$ , stress=100 bars). This is the input spectrum for hard rock conditions (~3000 m/s).

We can construct time histories of acceleration for the events by using the local geophone records as seed records, modifying them as needed to account for the

diminished geophone response at low frequencies, and to better match the target spectra of Figure 4. Spectral modification of the records is needed because they were recorded on high-frequency geophones, and therefore the natural frequency content of the records at frequencies less than about 8 Hz has been significantly filtered out. To minimize this problem to the extent possible, only the records from the 4.5 Hz geophones are used (i.e. we do not use records from the 14Hz geophones). The response of the 4.5Hz geophones is constant above 10 Hz, decaying slowly at lower frequencies (IMS, pers. comm. 2017); there is little significant energy recorded at frequencies less than 1 Hz. Thus we need to boost lower-frequency amplitudes to account for the instrument response and provide a reasonable match to the target spectrum. Note that the geophones record velocity, and thus a transformation to acceleration is also required.

The essence of the scaling approach is that we apply a frequency-dependent scale factor to the recorded waveforms, rather than a simple linear scale factor. This allows us to boost the lower frequencies in the record to account for instrument response, at the same time as we scale for distance; the distance scaling generally acts to reduce amplitudes because the recordings are at shorter distances than the target distance. The procedure is as follows. We take the Fourier transform of the velocity record, after applying zero-padding, baseline correction and tapering to ensure a well-behaved record. We then filter the record in the frequency domain to remove noisy components below 0.5 Hz. We also remove components above 200 Hz, which allows us to resample the records at a lower sampling rate. We decimate the records during processing so that the resampled records are at 600 samples/sec, compared to the input records as recorded at 6000 samples/sec. For the considered frequency range of 0.5 to 200 Hz, we modify the lower frequency components of the Fourier spectrum ( $< 8$  Hz) to correct for the instrument's amplitude response between 1 and 8 Hz; we then multiply the modified Fourier spectrum by the ratio of the target PSA spectrum to the recorded PSA spectrum of the modified input record (lightly smoothed). This ratio is frequency-dependent. The processing boosts the low frequencies whilst suppressing the higher frequencies as required, to bring the modified record to better agreement with the target spectrum. The inverse transform to the time domain provides the scaled time history.

The process is performed for each of the available seed records from the 4.5 Hz geophones, and the best 7 records are selected for each event, as judged by well-behaved time series, reasonable average scaling factor (0.2 to 5), and suitable match to the target. An overall scale factor (1.2) is also applied to all records to ensure that the target is met over the frequency range of interest (0.5 Hz to 20 Hz). Figure 5 shows the input and output spectra for the 2017 **M4.3** event in comparison to the target. Figure 6 shows the corresponding spectra for the 2018 **M3.0** events.

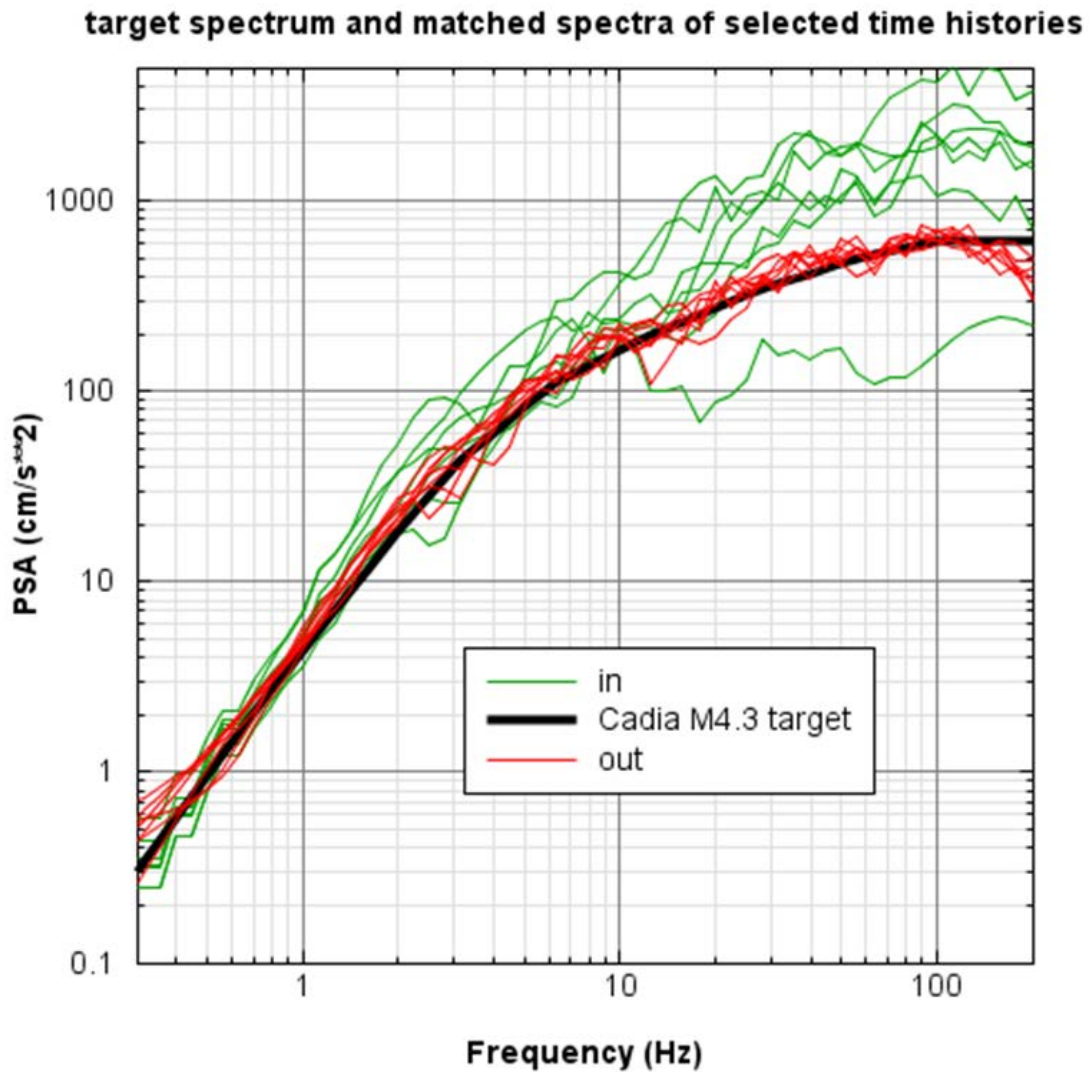


Figure 5 – Comparison of input spectra (green lines) to scaled spectra (red lines) for the 7 selected time histories for the 2017  $M=4.3$  event. The black line is the target spectrum (median plus sigma for  $M=4.3$  on hard rock at 5 km).

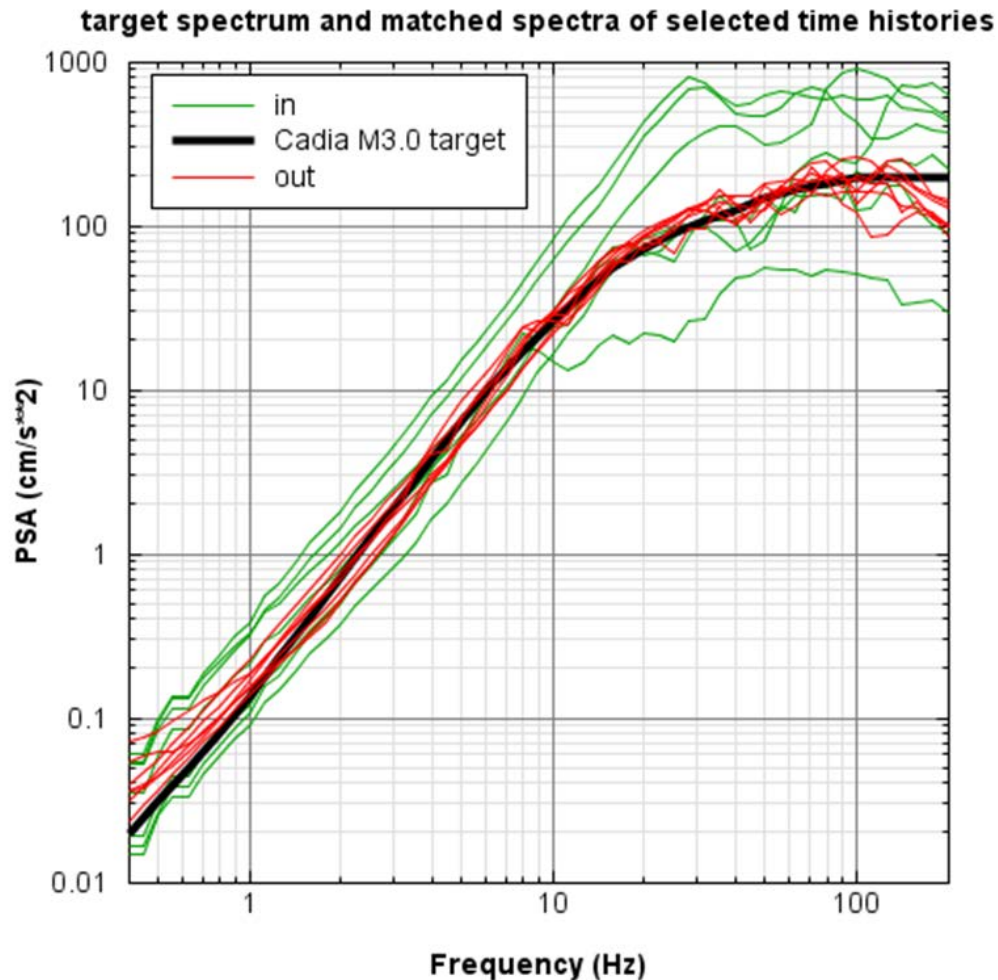


Figure 6 – Comparison of input spectra (green lines) to scaled spectra (red lines) for the 7 selected time histories for the 2018 **M**3.0 event. The black line is the target spectrum (median plus sigma for **M**=3.0 on hard rock at 5 km).

The scaled time histories are very similar in overall character to the original records in the time domain but have modified amplitudes and frequency content. A limitation of the time series is that they have little frequency content below 1 Hz, because of the instruments that recorded them. However, as can be seen in Figures 5 and 6, the target spectra also have very little energy content at < 1 Hz. The appendices show the 7 records for each event set, in which the seed velocity input is also displayed. An example is given in Figure 7 for the **M**4.3 event, with a different example given in Figure 8 for the **M**3.0 event. Note that the time series for the **M**3.0 event are for either the first or second of the events; file f46 is one of the records from the first event, whilst the other selected records are from the second event.

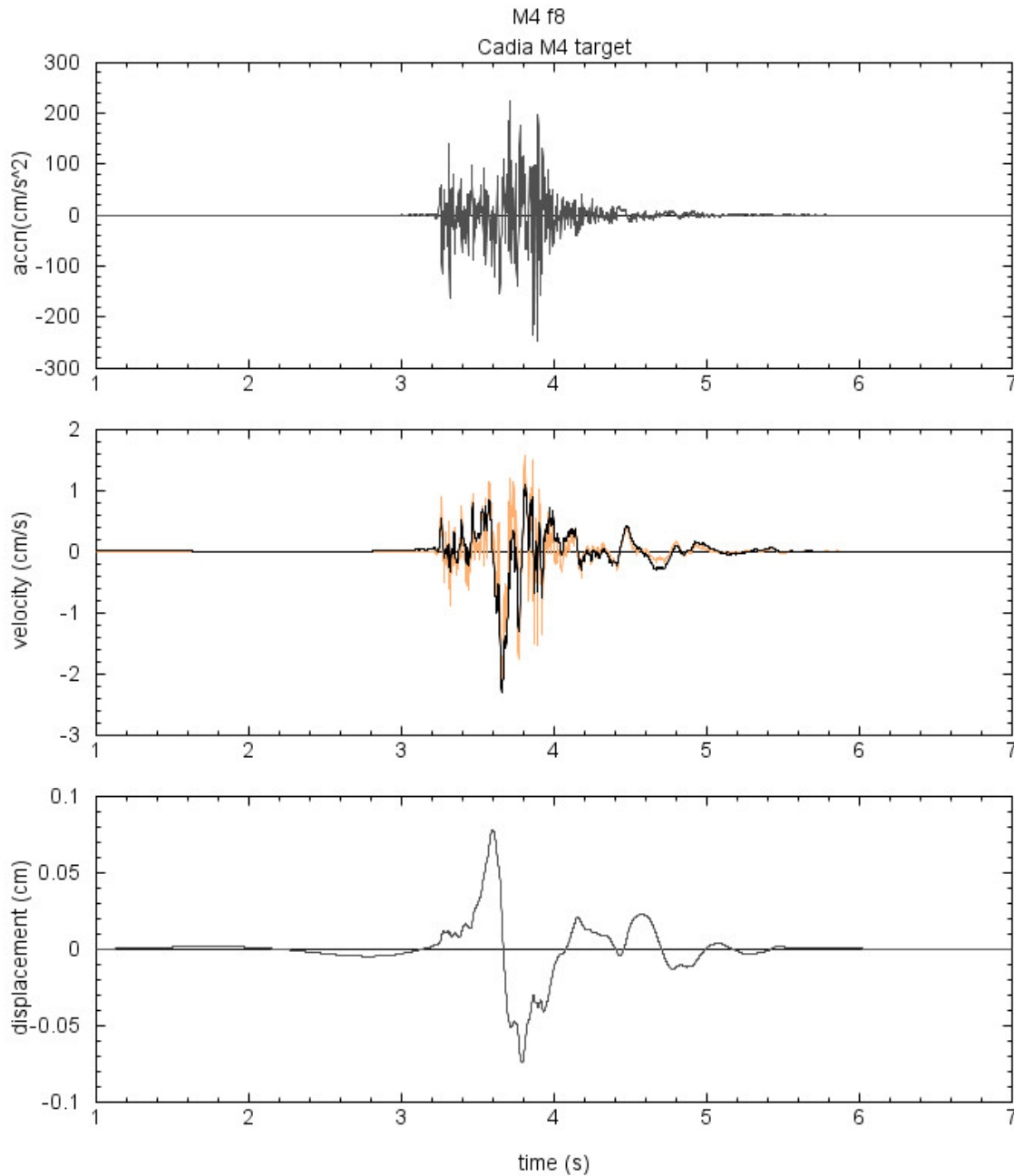


Figure 7 – Example of scaled time histories for the 2017 **M4.3** event (file f8). The input velocity record is shown in orange. Black lines are the scaled acceleration (top), velocity (middle) and displacement (lower) records.

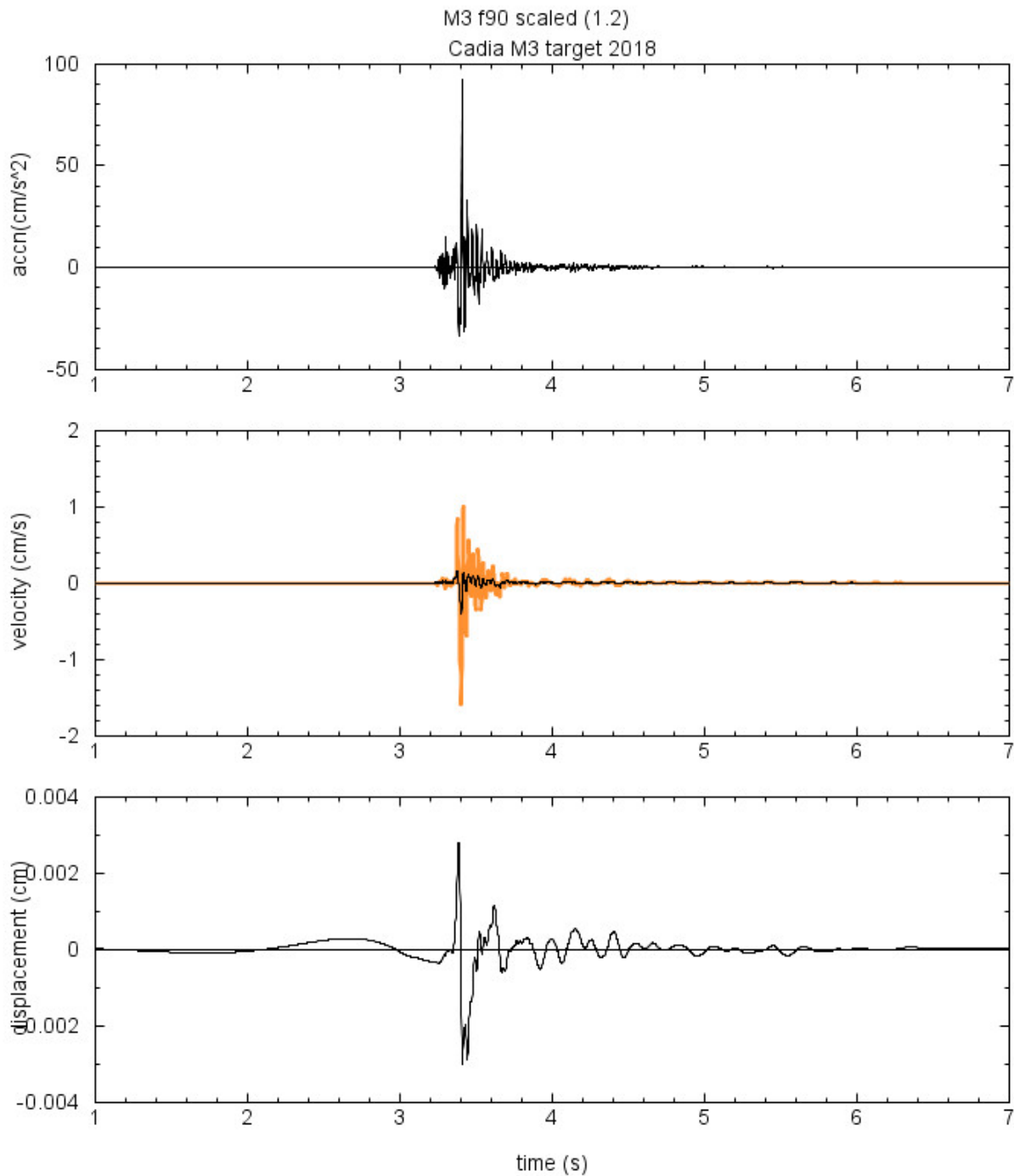


Figure 8 – Example of scaled time histories for the 2018 **M3.0** event (second of the two closely-spaced events) (file f90). The input velocity record is shown in orange. Black lines are the scaled acceleration (top), velocity (middle) and displacement (lower) records.

The ML3.5 event of Nov. 25, 2017 was not analyzed. However, based on its intermediate magnitude, its spectrum and ground motions would be intermediate to those of the **M3.0** and **M4.3** events – about half-way between in log space. Thus approximate time series could be constructed by using the **M4.3** records, and dividing all amplitudes by a factor of three (i.e. see Figure 4). Cumulative effects of multiple events occurring in a sequence are discussed in the next section. All time series are for input at hard rock site conditions (shear wave velocity ~3000 m/s) beneath any soil layers.

The bedrock time series (containing the output acceleration, velocity and displacement, as well as the raw input velocity, all in cgs units) are provided in digital ascii files, at 600 samples/sec. The ascii time series files are named in the format f\*.M4d3.out for the **M4.3** event and f\*.M3d0.out for the **M3.0** event.

## **Additional Analyses and Considerations**

### **July 22, 2018 M3.1 Event**

Following the initial analyses of these events, there was an additional significant event that occurred on-site July 22, 2018, listed as local magnitude ML=3.8 by Geoscience Australia. Figure 9 shows the location of this event and recording stations. In addition to the instruments that recorded the March 2018 events, there are two additional instruments in place for this event: a 4.5 Hz geophone at the South Tailing Dam (on the embankment wall) and a broadband seismometer (Trillium compact posthole by Nanometrics), buried in about 1 m of soil, about 1 km from the failure site. These instruments are at distances of 6 to 7 km from the source. IMS provided the velocity records as recorded on-site, corrected for gain. Regional records were obtained from IRIS. An analysis of the ground motions from this event was undertaken as described in the following and used to develop an additional 3-component record set to represent the March **M3.0** event as experienced at the failure site, at the input bedrock level. All records were processed as described for the earlier events.

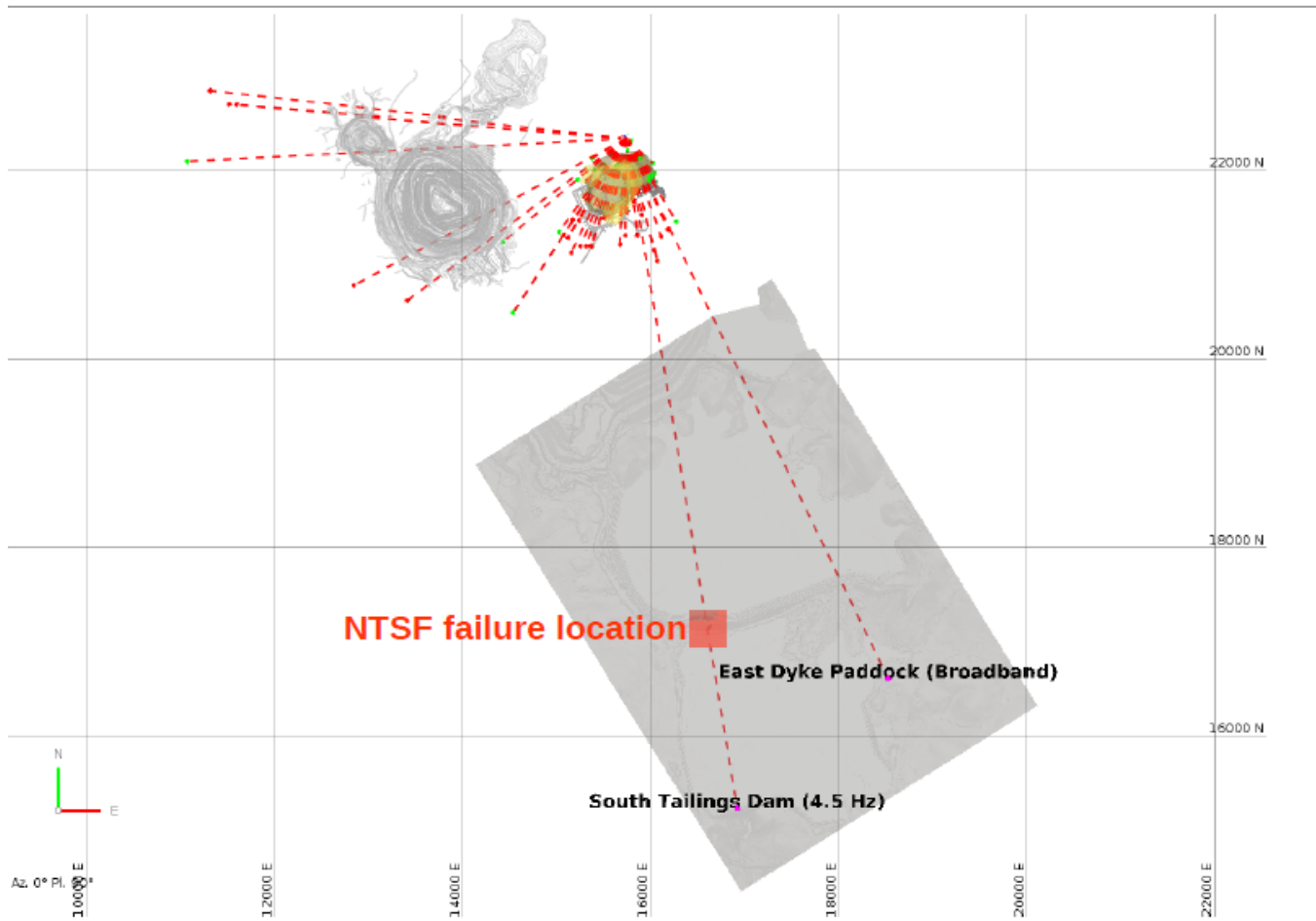


Figure 9 – Location of  $M3.1$  July 22, 2018 event (red dot) and recording stations (dots at end of red rays) (from IMS, 2018b).

Figure 10 compares the response spectral amplitudes of the July 2018 event to those of the earlier events. At regional distances ( $>100$  km) the motions of the July 2018 event were significantly larger than those for the March 2018 events, which explains the  $ML=3.8$  magnitude obtained by Geoscience Australia for the event. On-site, however, the motions for the July and March events appear to be very similar in amplitude across a broad range of frequencies. Considering the 1-Hz PSA values on-site, in comparison to the hard-rock GMPE model of Hassani and Atkinson (2018), the moment magnitude of the July 2018 event is estimated as  $M=3.1$ , though based on the regional amplitudes it is possible it was larger (as great as  $M=3.5$ ). Note that the motions plotted at 6 km (the broadband site) and 7 km (the South Tailings site) do not represent hard rock motions. The broadband site is a 1 m burial in soil, whilst the South Tailings site is on the wall of the tailings embankment (Denver Birch, IMS, pers. comm. Sept. 2018). Considering the similarity of amplitudes on-site for the March and July 2018 events, the broadband recordings obtained at the

broadband and South Tailings sites for the July 2018 are excellent analogues for what was likely experienced there in March 2018.

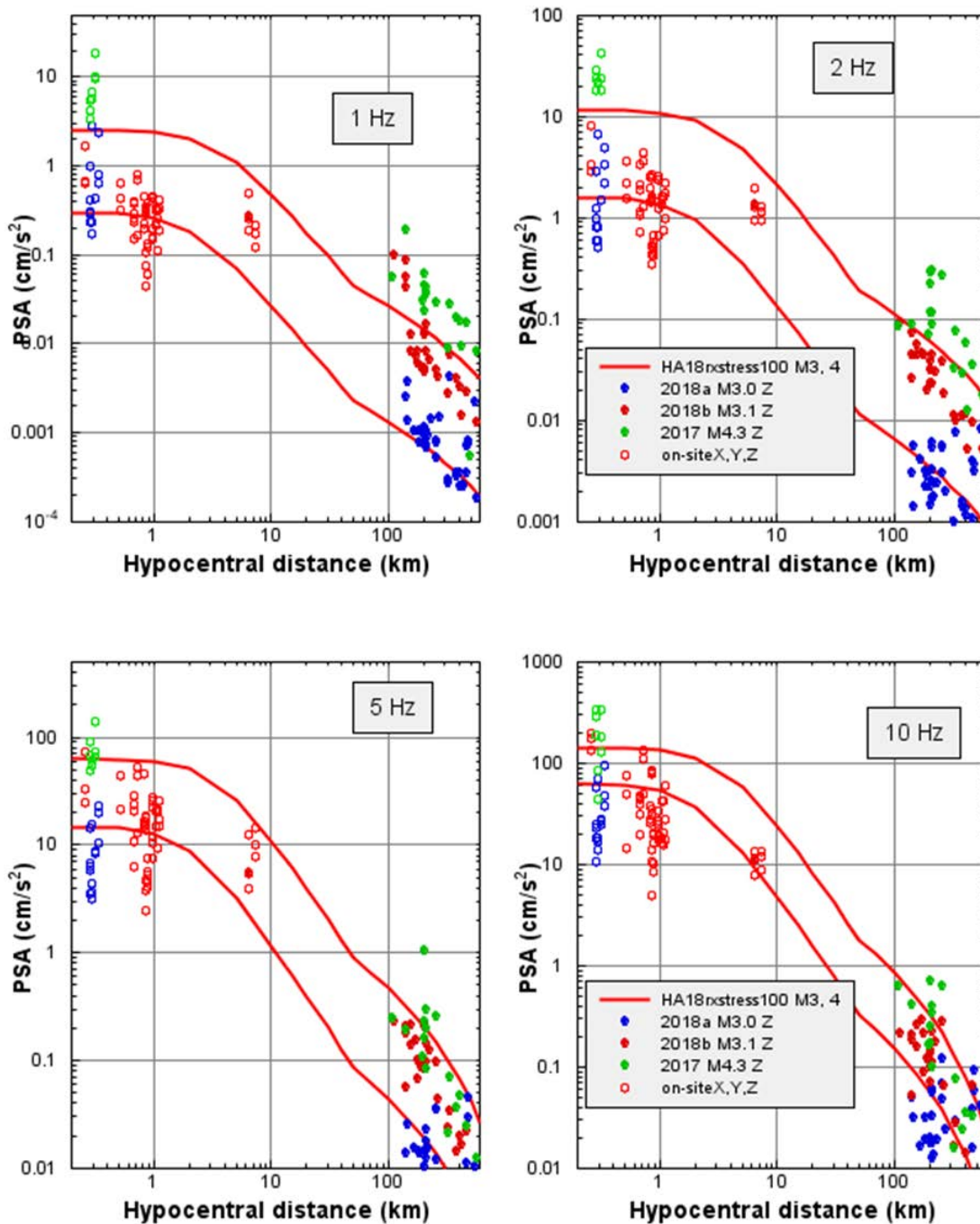


Figure 10 – Comparison of response spectral amplitudes for the July 2018 **M3.1** event (red dots) with those for the **M3.0** March 2018 events (blue dots) and the **M4.3** April 2017 event (green dots). For regional stations (>100 km) only the vertical components are plotted. For on-site stations, the geometric mean as given by IMS is plotted for the 2018a and 2017 events, whilst all three components are plotted for the July 2018

*event. Red lines show the hard-rock GMPE of Hassani and Atkinson (2018) for  $M=3$  and  $M=4$ . Note that the stations at distances  $> 2$  km are not sited on rock.*

Figure 11 examines the response spectra recorded at the broadband and South Tailings sites, near the ground surface, in comparison to the range of recorded motions on rock within the mine, closer to the source. It is observed that the in-mine motions for the July event are very close to the spectrum defined as the target for the **M3.0** March event. The motions recorded near the surface at both the broadband and South Tailings sites are also very similar to the **M3.0** target, for frequencies up to about 8 Hz. At higher frequencies, the broadband and South Tailings records have lower amplitudes, likely attributable to the effects of burial in near-surface soil. The deficiencies of these records at higher frequencies, as analogues to the input-level motions on rock at greater depth, can be addressed by using the same frequency-dependent scaling approach that was applied to the other records, employing the same **M3.0** target. As seen in Figure 11, when this procedure is applied to the broadband records, they match the target well for frequencies up to 30 Hz. Some deficiencies remain at very high frequencies, but these are not likely to be of practical importance. The additional scaled time series based on the broadband records of the July 2018 event, representing likely input motions on rock for the March 2018 event, are provided in ascii format in digital files f38BB\*r.out, where \* is 1, 2, 3 for the x, y and z components, respectively. Figure 12 provides an example of these records.

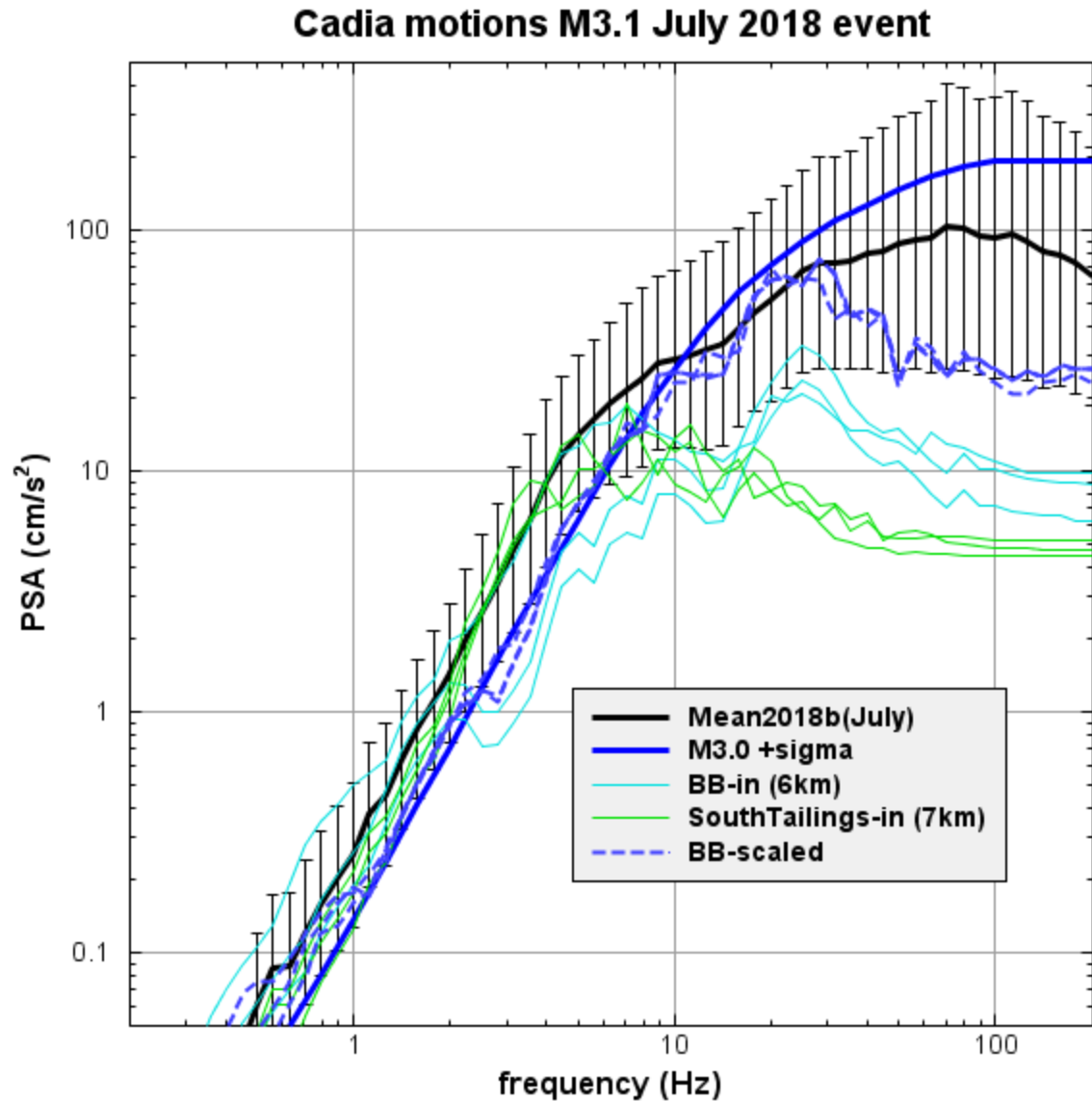


Figure 11 – Motions recorded near-surface at the broadband (light blue) and South Tailings (green) sites in comparison to the mean of motions recorded in the mine on rock for the event (black line, error bars show standard deviation, sigma). The target spectrum for the **M3.0** March 2018 event, as defined earlier is shown (solid blue). The broadband motions after scaling to the target are shown in dashed blue lines.

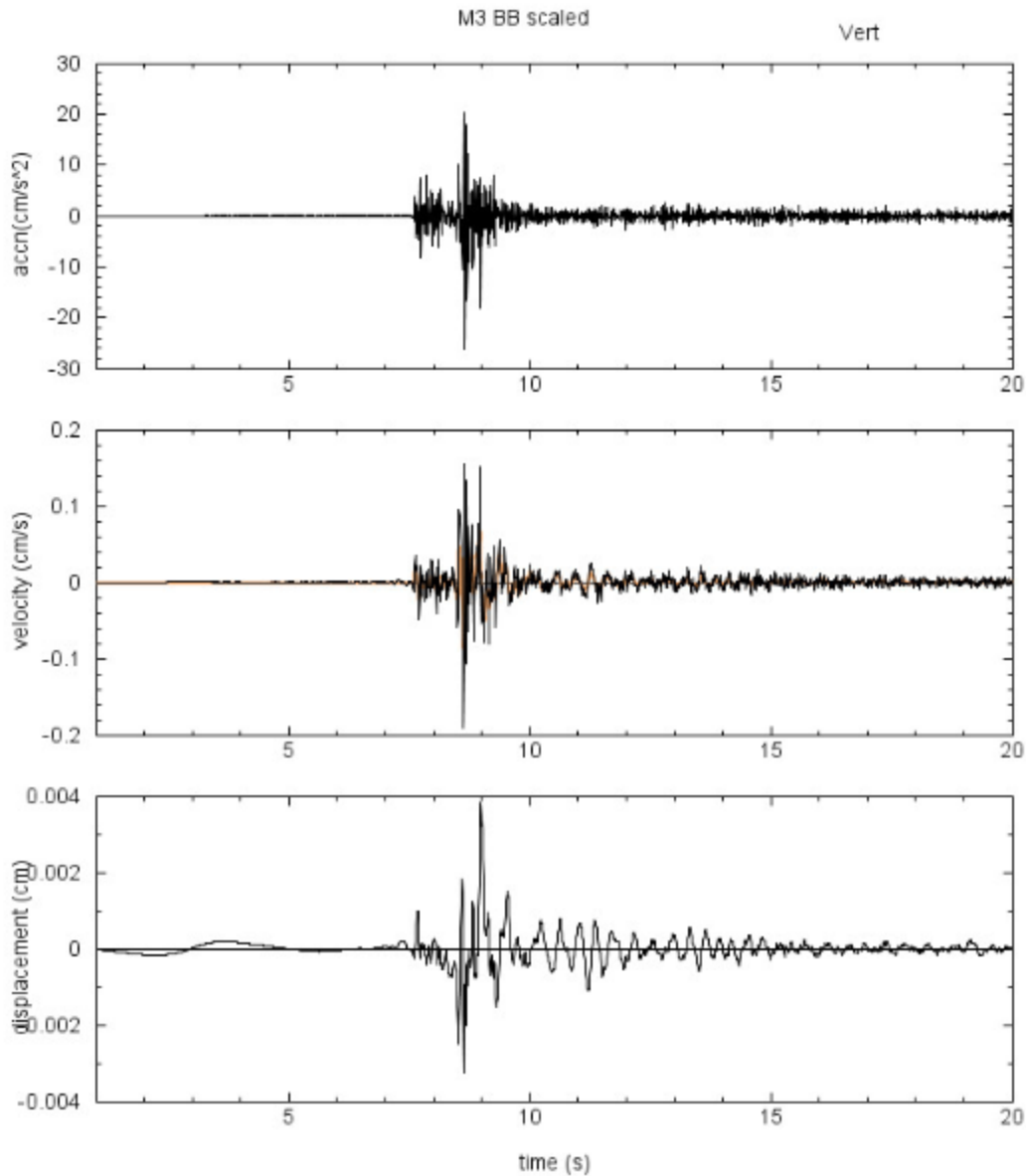


Figure 12 - Scaled time histories for the July 2018 **M3.1** event (file *f38BB3r.out*). The input velocity record is shown in orange (beneath scaled output, very similar). Black lines are the scaled acceleration (top), velocity (middle) and displacement (lower) records.

### *Cumulative Effects of Multiple Events*

A consideration that may be significant is that the Cadia site experiences relatively-frequent low-level seismicity, and there might be cumulative effects over many small events. For the March 2018 events, the two **M3.0** events occurred right after each

other (origin time delayed by only 10 sec). Therefore for each deformation analysis for this event two records should be input to the structures in series.

In the one-year period from April 2017 to March 2018 there were 4 events of  $M > \sim 3.0$  (April 2017, Nov. 2017 and March 2018). If the deformations from these events might be cumulative, then a sequence of four significant time series, constructed using the records provided in the previous section, could be input to the structure in series to investigate the potential effects. In such an exercise, note that only the last two  $M 3.0$  events were very close together in time

It should also be considered that there are many smaller events ( $M < 3$ ) associated with the larger events. For example, there were many aftershocks recorded in the 12 hours following the  $M 4.3$  event of April 2017, as illustrated in Figure 13. Based on the Gutenberg-Richter relation we would expect that for each  $M \sim 4$  event in a sequence there may be  $\sim 10$   $M \sim 3$  events. Similarly, for each  $M \sim 3$  event in a sequence there may be  $\sim 10$   $M \sim 2$  events. None of the aftershocks shown on Figure 13 was of  $M > 3$ , based on catalogue records. Thus the deformation effects of the aftershocks would be less than those of the provided records for the  $M 3$  events. However, if there is impact from the  $M 3$  events, then it may be warranted to consider whether dozens of very small events would be consequential. For example, one might consider  $\sim 20$  events occurring over a few hours, each with amplitudes about  $1/10^{\text{th}}$  of those of  $M 3$  events.

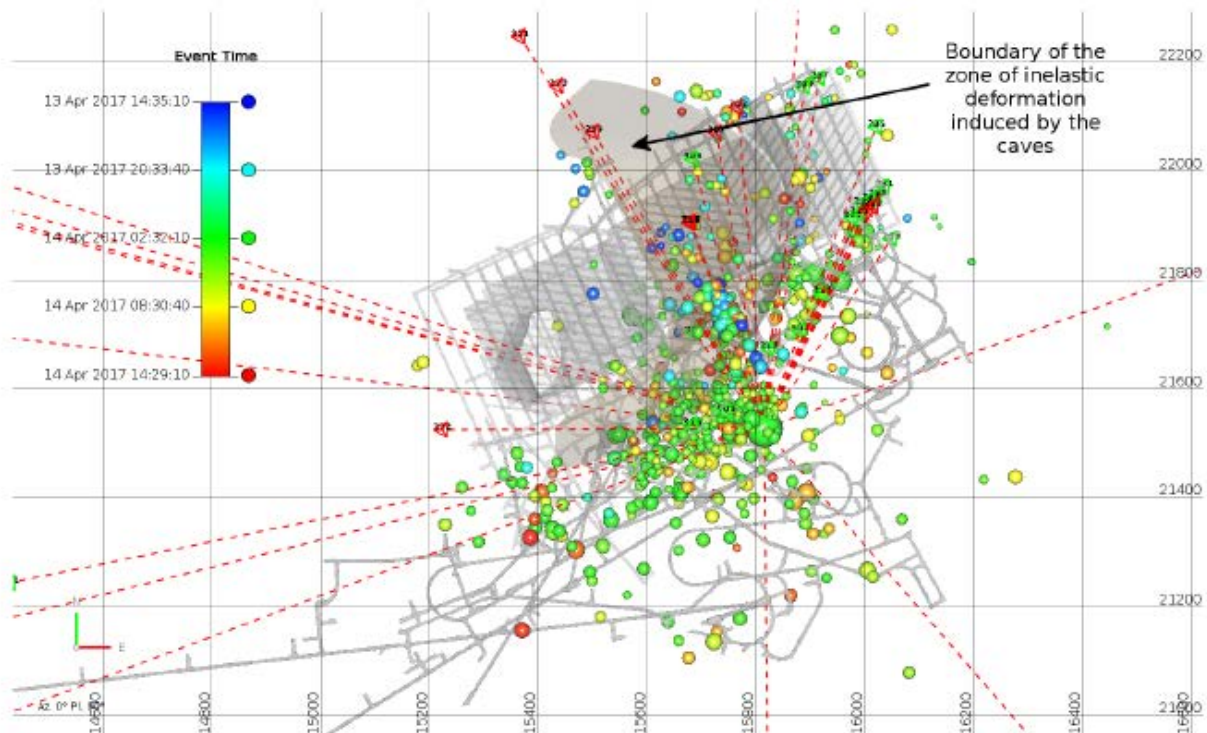


*Figure 13 – Distribution of events recorded within  $\pm 12$  hours of the April 2017 **M**4.3 event. Circle sizes represent relative event sizes. Rays show paths towards recording stations from mainshock (from IMS, 2017).*

### *Effects of Uncertainty and Site Amplification at the failure site*

The motions provided are to be input at the bedrock level (shear-wave velocity  $\sim 3000$  m/s). These input motions are subject to both epistemic and aleatory uncertainty, which is likely to be near a factor of two. In addition, the input motions would be amplified significantly by underlying soil deposits. Site response effects can be very large for weak motions, especially if the failure site is underlain by soil deposits that have a predominant natural period in the range of interest for the embankment. Resonant soil response amplifications of as much as a factor of 5 to 10 are possible if there is a soil layer underlain by a significant impedance contrast (e.g. Hassani and Atkinson, 2017). On the other hand, soft soils near surface can also act to attenuate high-frequency motions. The effects of site response on the input bedrock motions at the site of the embankment should be carefully evaluated based on the site geotechnical profile.

To reduce the uncertainty in the ground motions that occurred at the failure site, it is recommended to maintain and calibrate one or more broadband seismometers at or near the failure site. Future small earthquakes could then be used to more confidently determine the relationship between motions observed at the monitoring stations that recorded the previous events (i.e. the mine network of geophones) and the actual motions at the failure site.

### **References**

- Assatourians, K., and G. Atkinson (2010). Database of processed time series and response spectra for Canada: An example application to study of the 2005 MN5.4 Riviere du Loup, Quebec earthquake. *Seism. Res. L.*, **81**, 1013-1031.
- Atkinson, G. (2015). Ground-motion prediction equation for small-to-moderate events at short hypocentral distances, with application to induced seismicity hazards. *Bull. Seism. Soc. Am.*, **105**, doi: 10.1785/0120140142.
- Atkinson, G., D.W. Greig and E. Yenier (2014). Estimation of moment magnitude (**M**) for small events ( $M < 4$ ) on local networks. *Seism. Res. L.*, **85**, 1116-1124.
- Atkinson, G., B. Hassani, A. Singh, E. Yenier and K. Assatourians (2015). Estimation of moment magnitude and stress parameter from ShakeMap ground-motions. *Bull. Seism. Soc. Am.*, **105**, 2572-2588.

Hassani, B. and G. Atkinson (2017). Site-effects model for central and eastern North America based on peak frequency and average shear-wave velocity. *Bull. Seism. Soc. Am.*, **107**, doi: 10.1785/0120170062.

Hassani, B. and G. Atkinson (2018). Adjustable Generic Ground-Motion Prediction Equation Based on Equivalent Point-Source Simulations: Accounting for Kappa Effects. *Bull. Seism. Soc. Am.*, **108**, doi: 10.1785/0120170333.

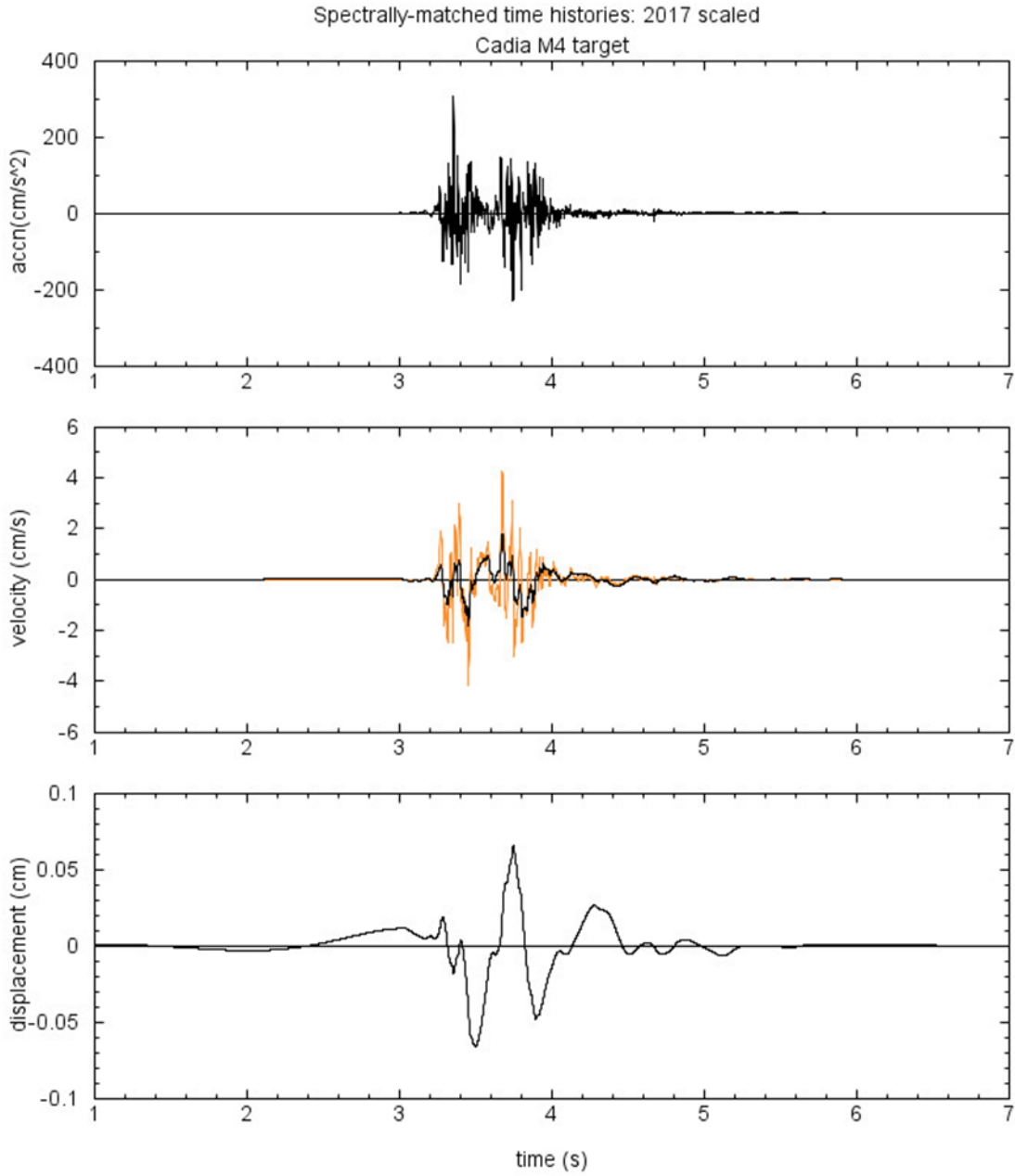
IMS (2017). Cadia East Mine: Analysis of large seismic event on 14 April 2017. Institute of Mine Seismology, Rpt CAD-REP-LRGEVENT-20170414-IMS.

IMS (2018). Cadia East Mine: Probabilistic Assessment of Mining-induced ground motion hazard for the Northern Tailings Storage Facility. Institute of Mine Seismology, Rpt CAD-NOTE-PSHA4NTSF-201803-IMS.

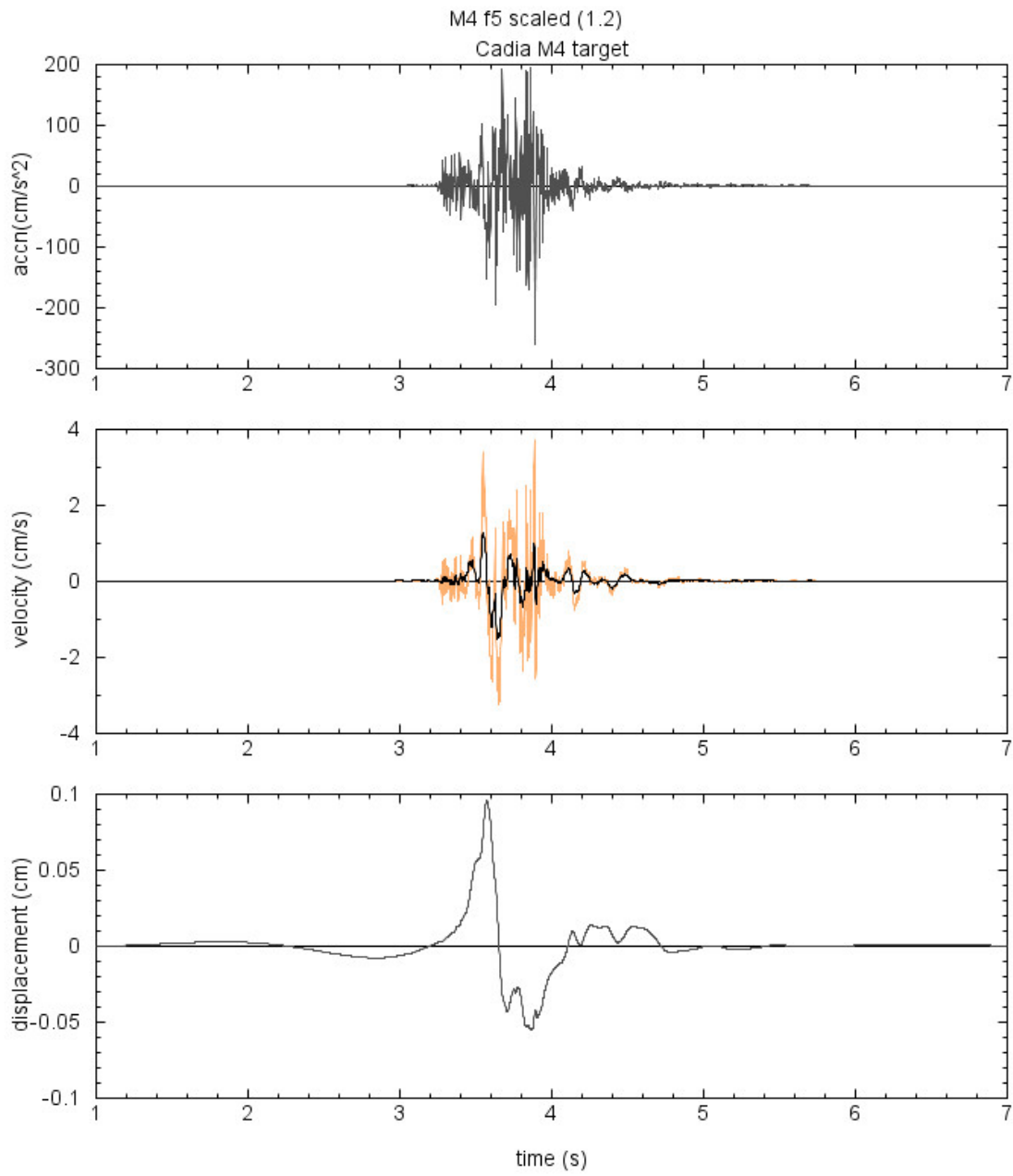
IMS (2018b). Cadia East Mine: Brief results of analysis of large seismic event at Cadia East mine recorded on 22 Jul'18 at 12:46:00. Institute of Mine Seismology, Rpt CAD-NOTE-LRGEVENT-20180722-IMSv5.

Novakovic, M., G. Atkinson and K. Assatourians (2018). Empirically-calibrated ground-motion prediction equation for Oklahoma. *Bull. Seism. Soc. Am.*, **108**, in press.

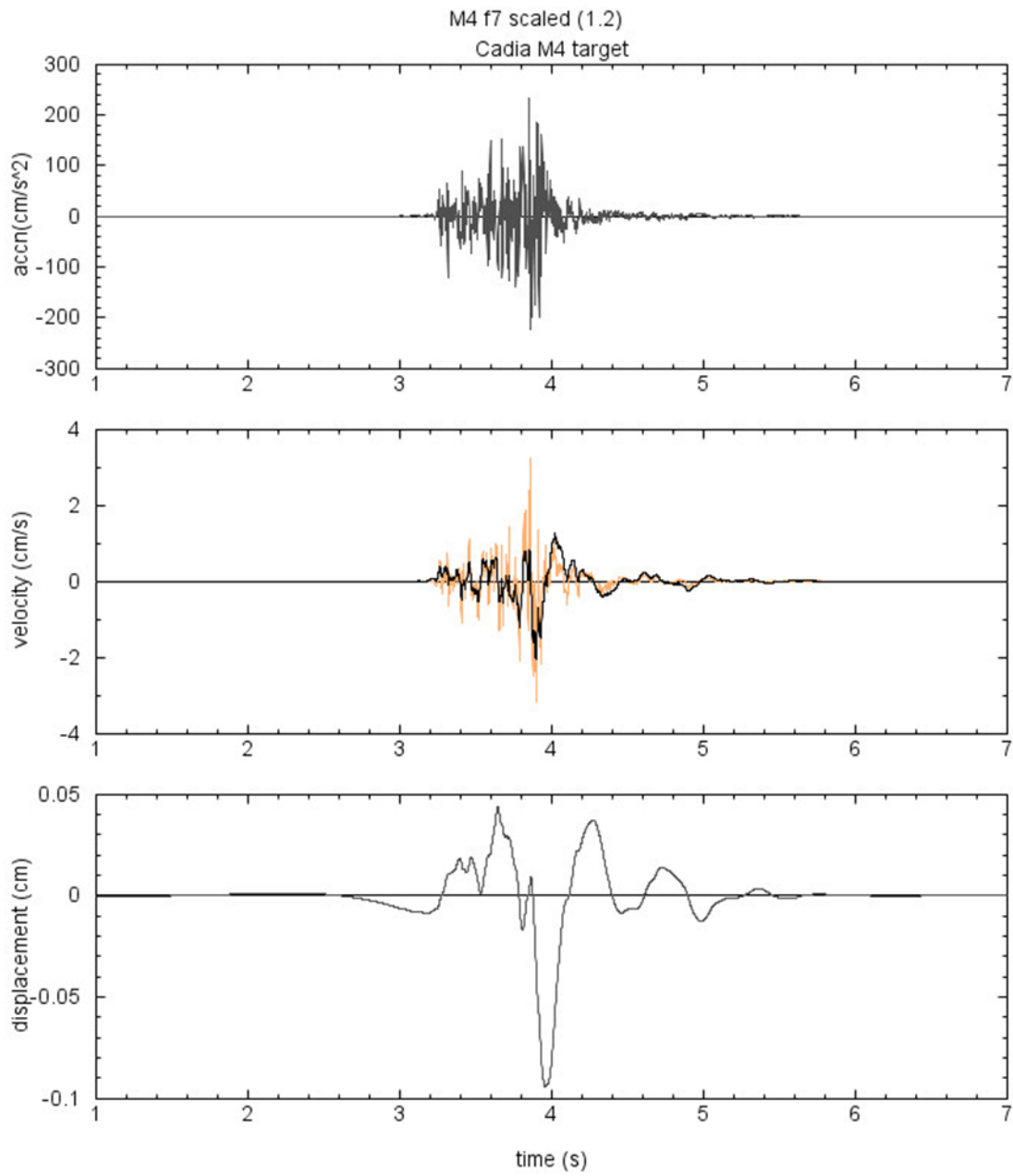
**Appendix A – Time Series Plots for M4.3 (files f1, f5, f7, f8, f9, f10, f11, f24)**



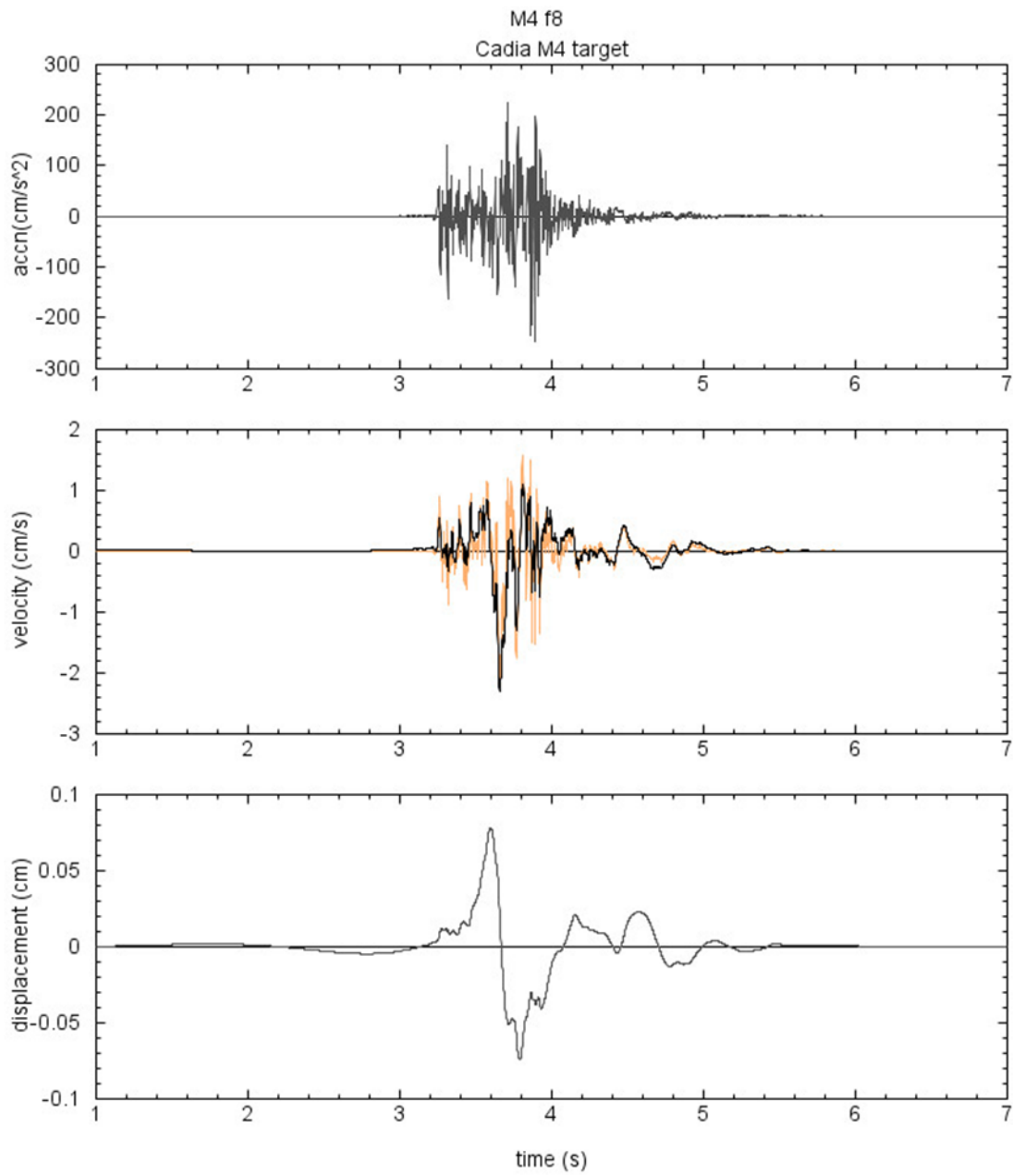
M4 f1



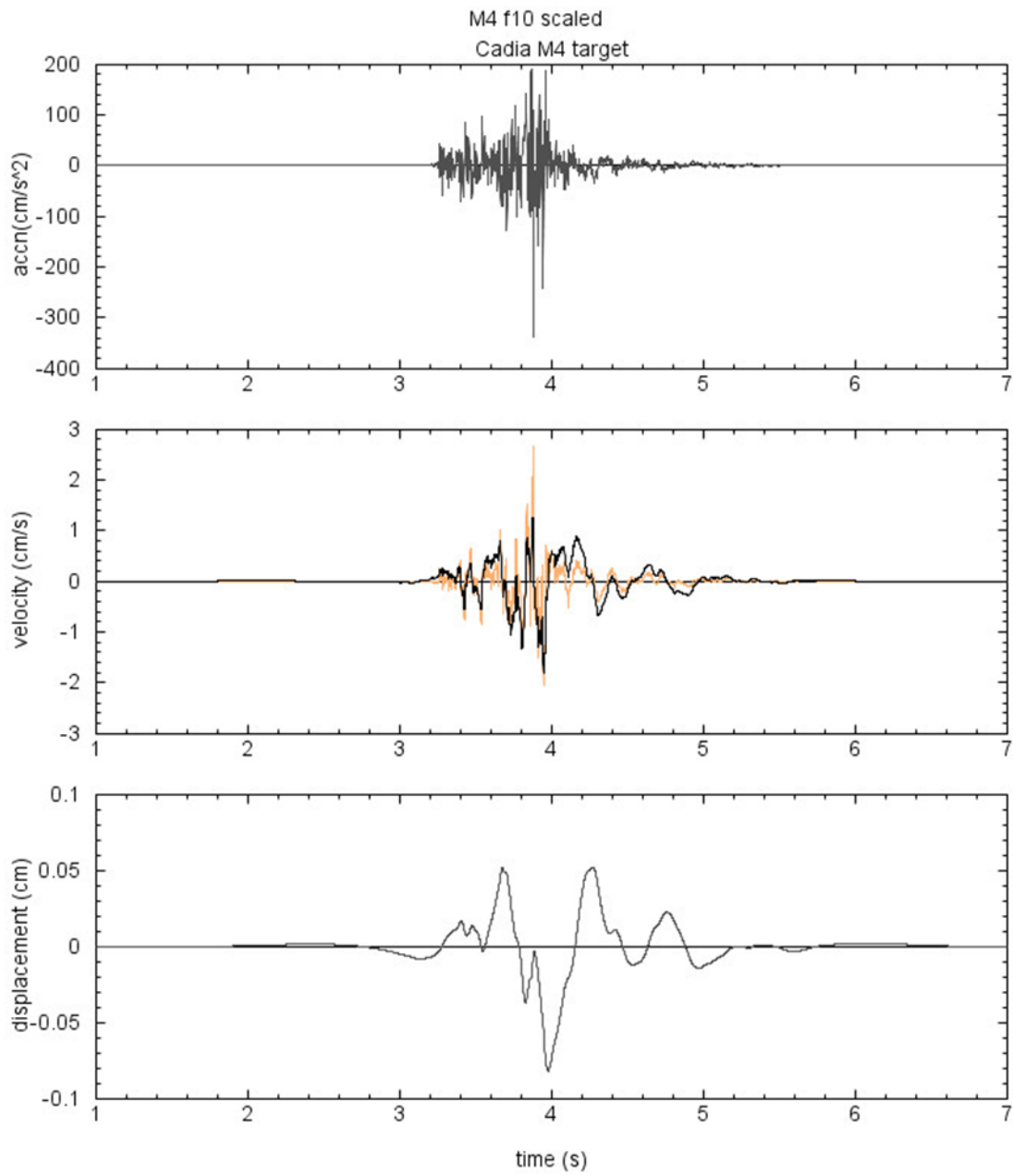
M4 f5



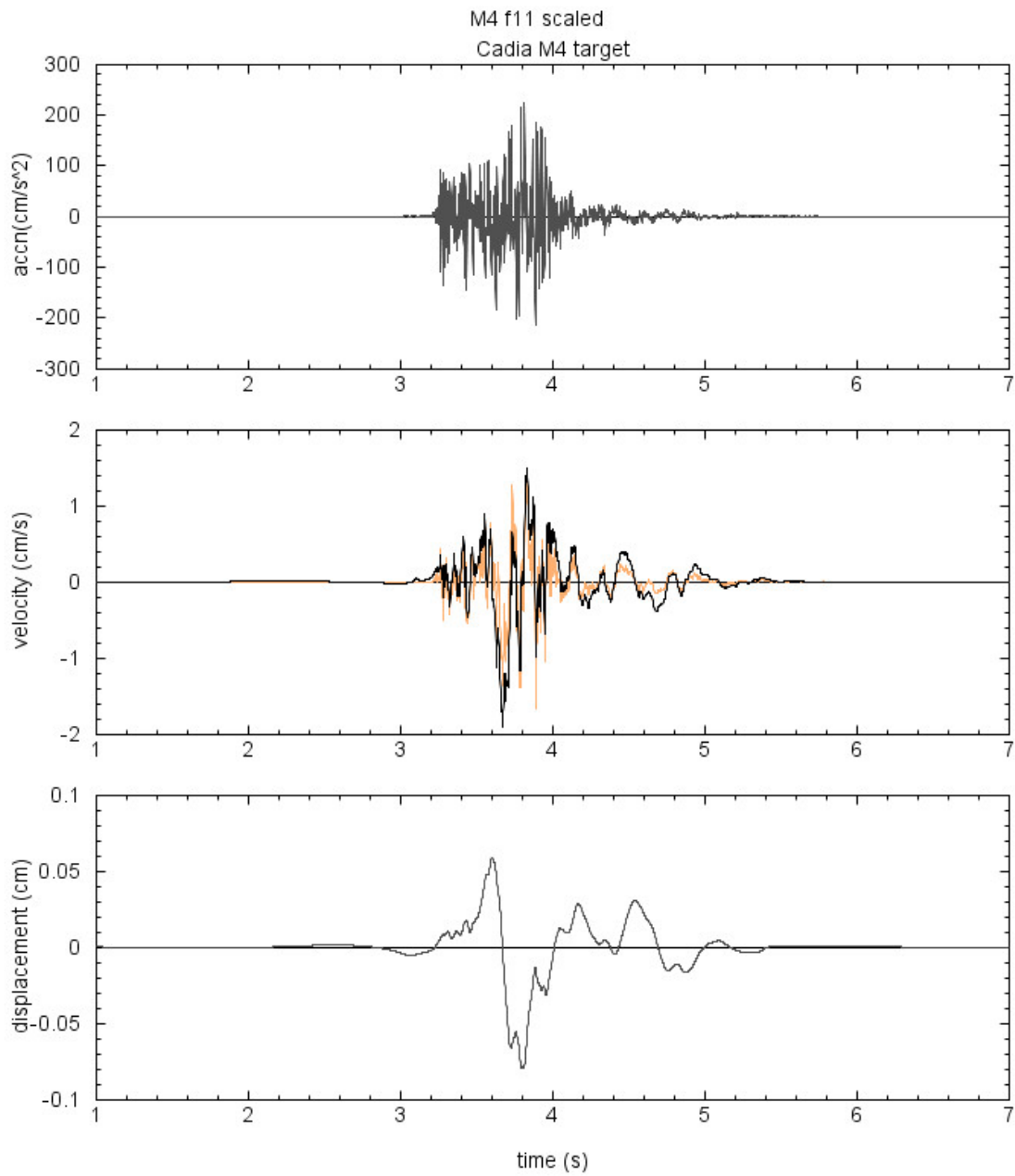
M4 f7



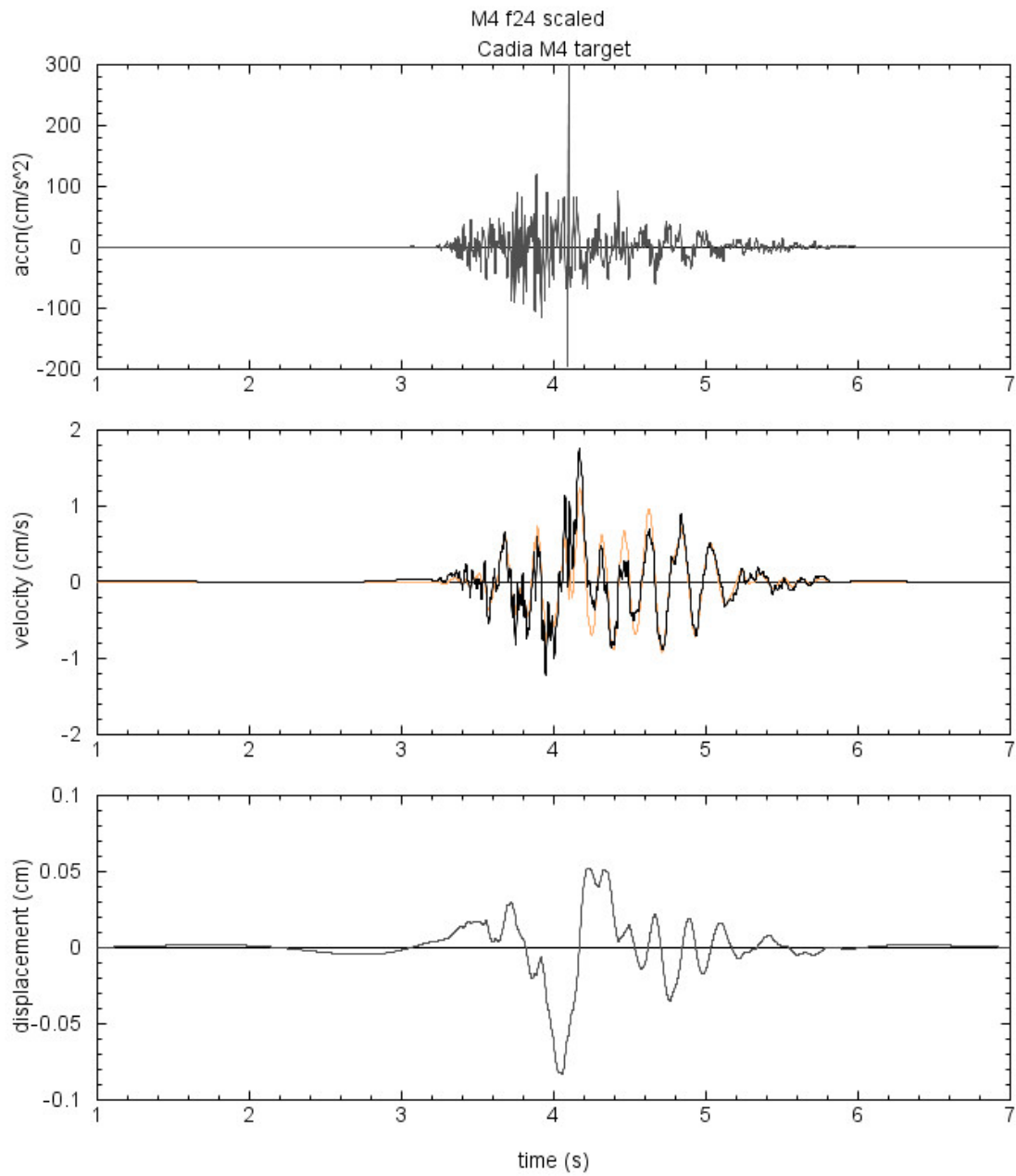
M4 f8



M4 f10

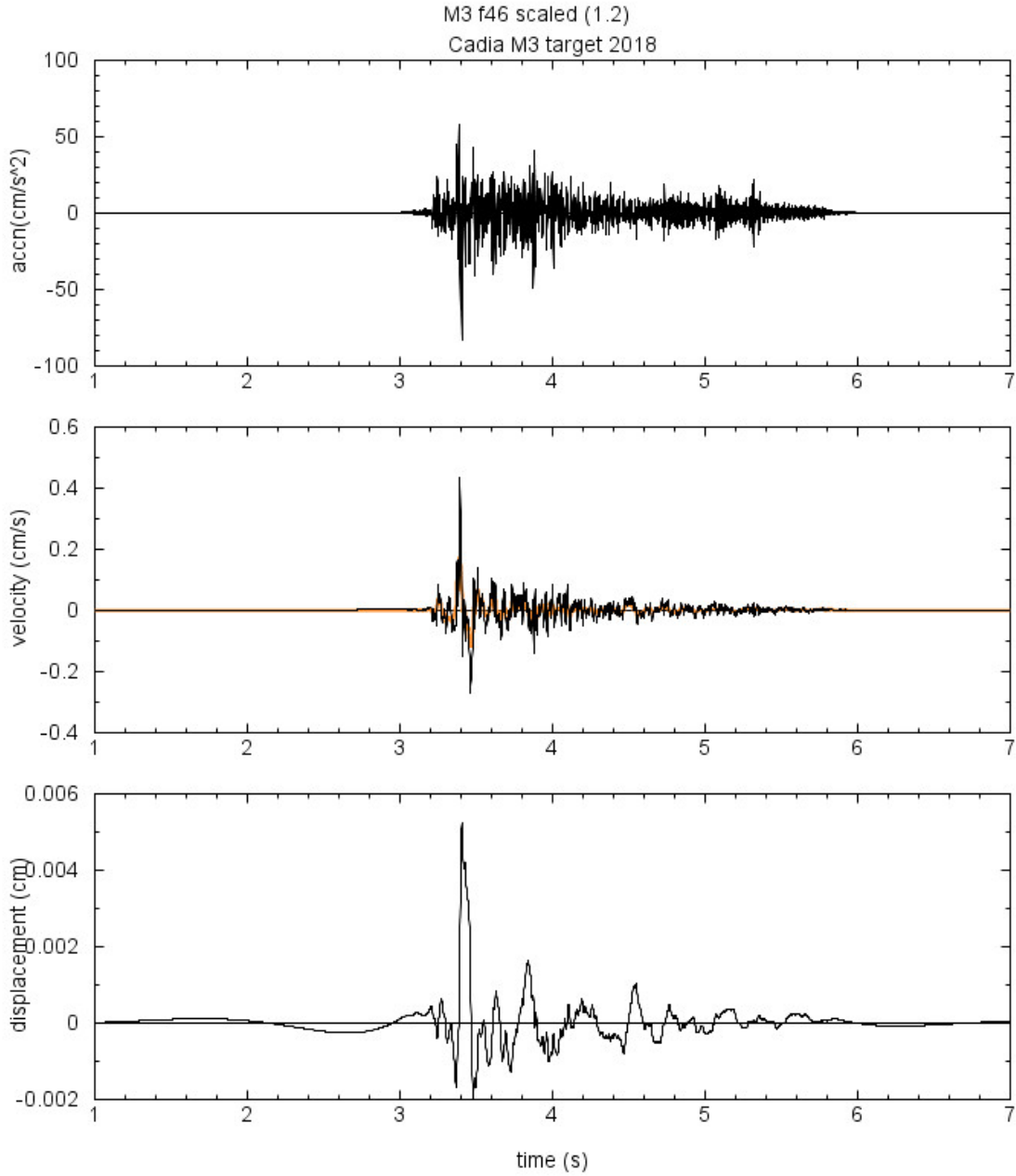


M4 f11

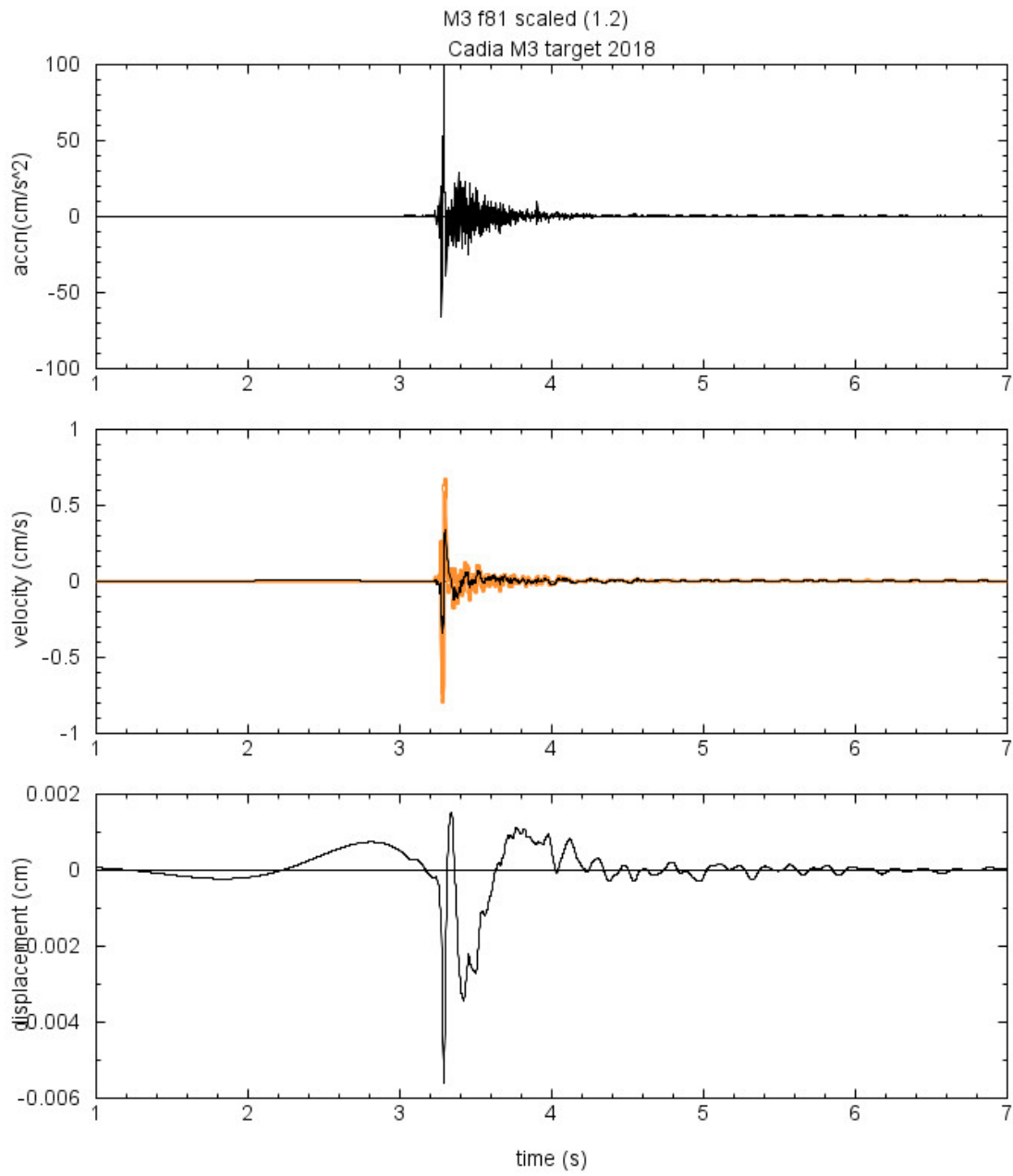


M4 f24

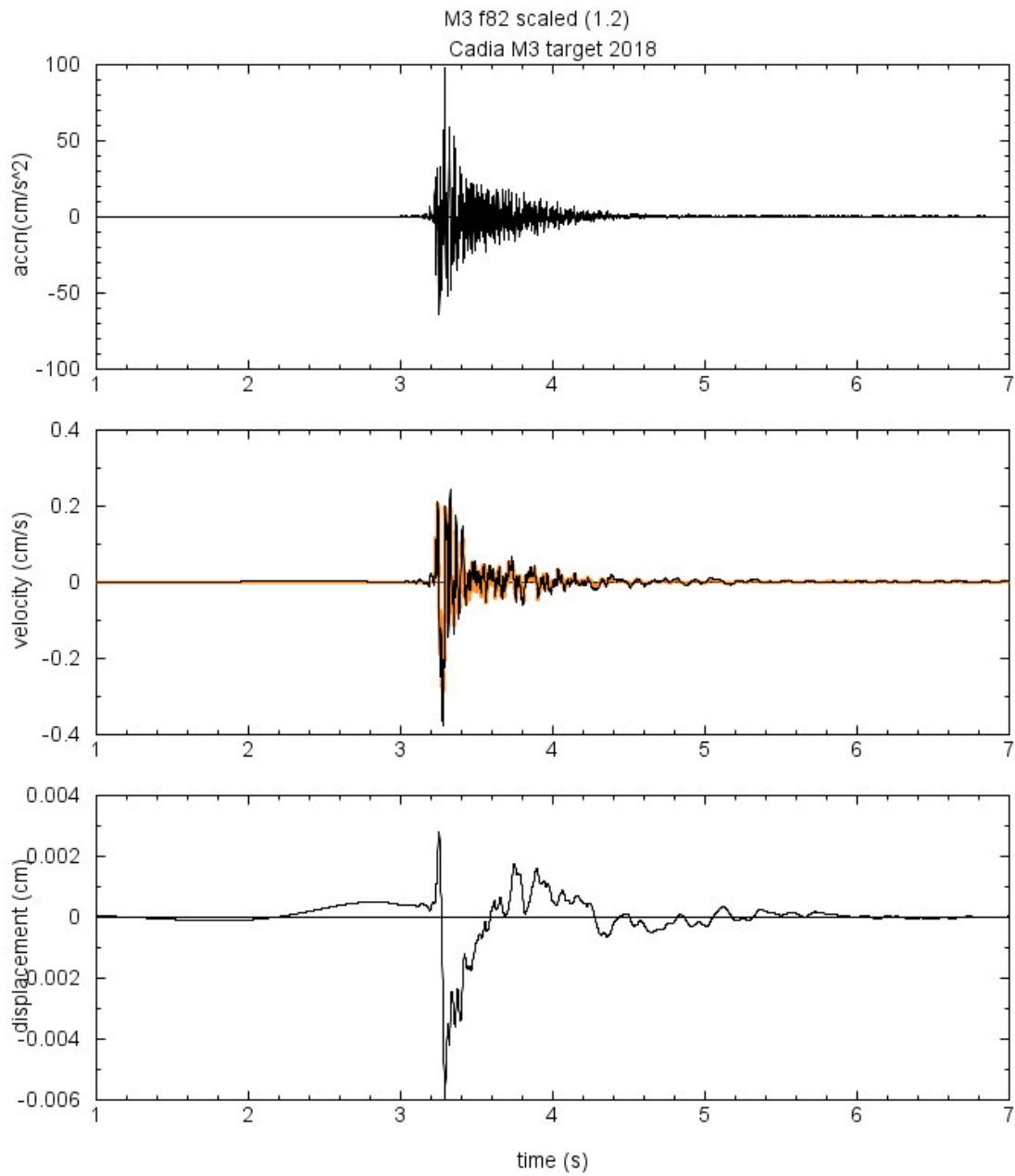
**Appendix B – Time Series Plots for M=3.0 (files f46, f81, f82, f83, f90, f91, f92)**



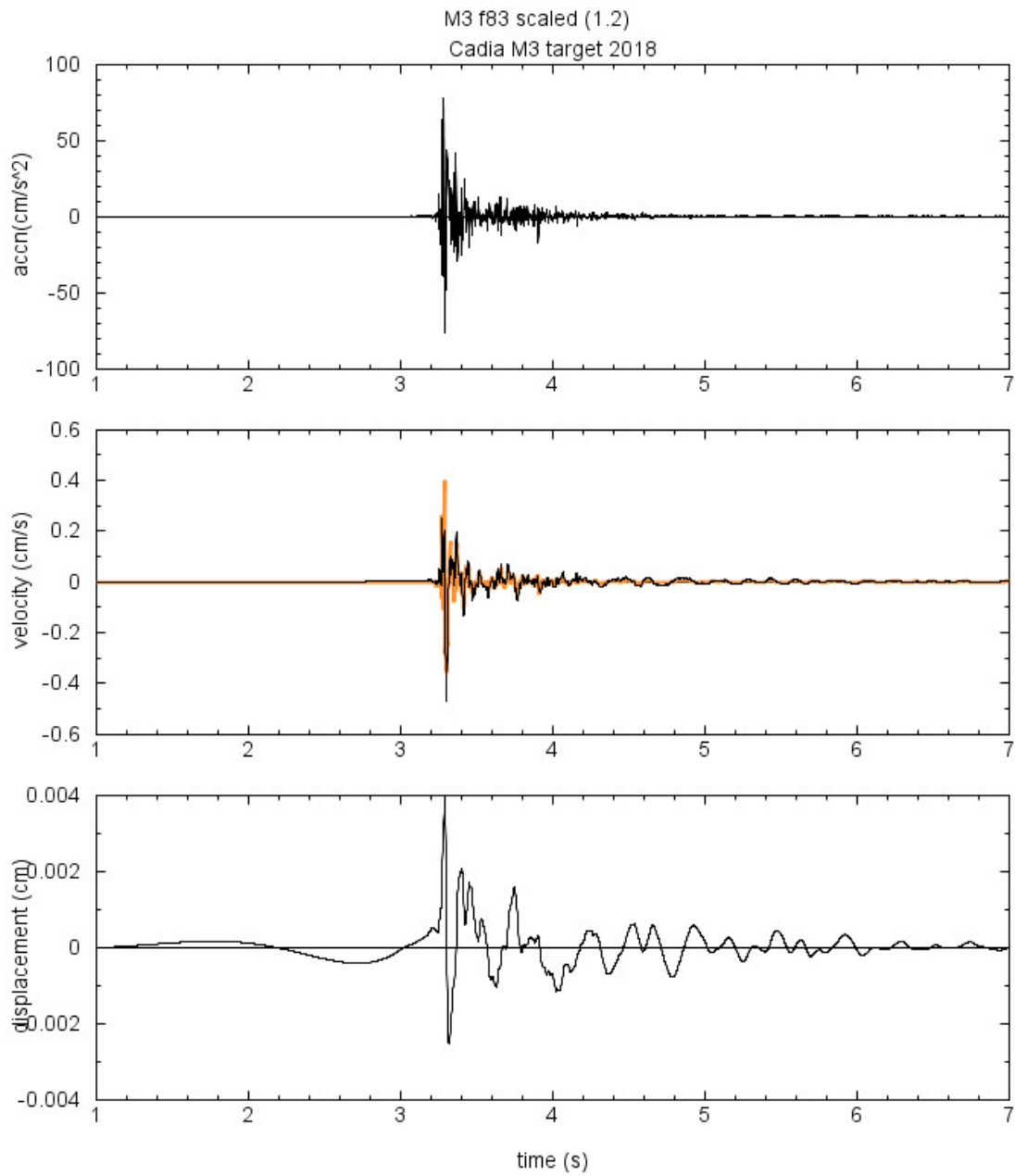
M3 f46 scaled (1.2)



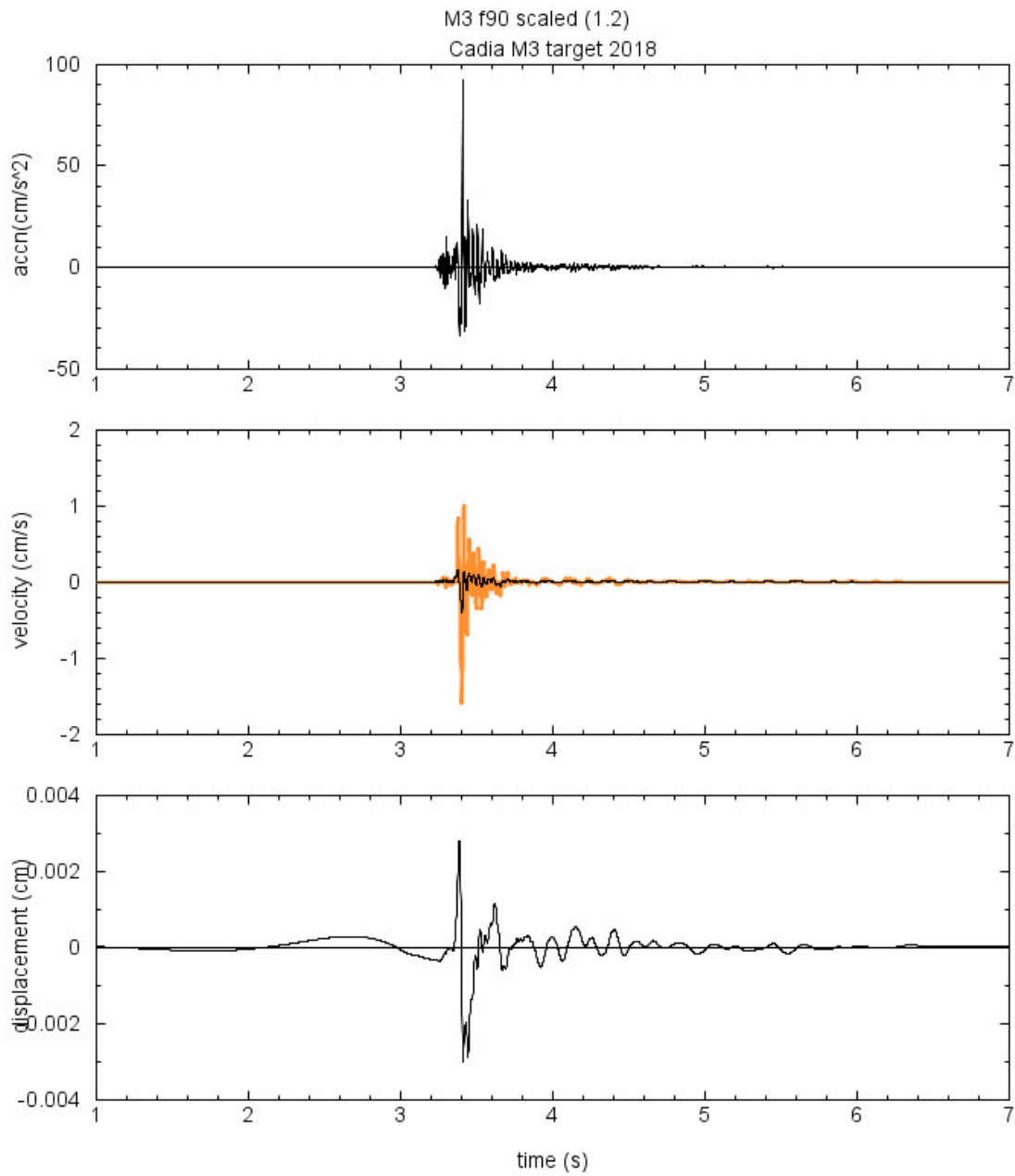
M3 f81 scaled (1.2)



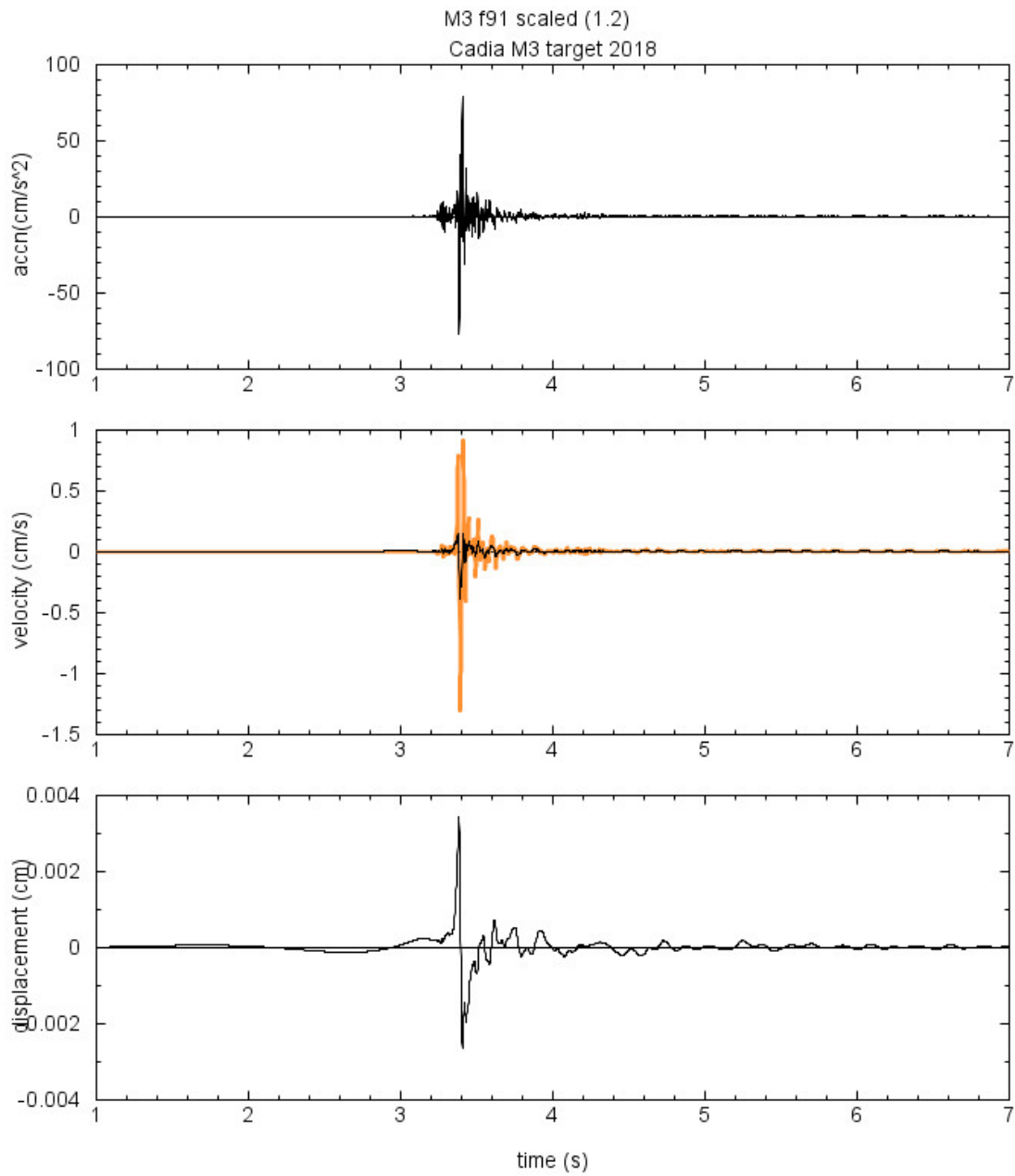
M3 f82 scaled (1.2)



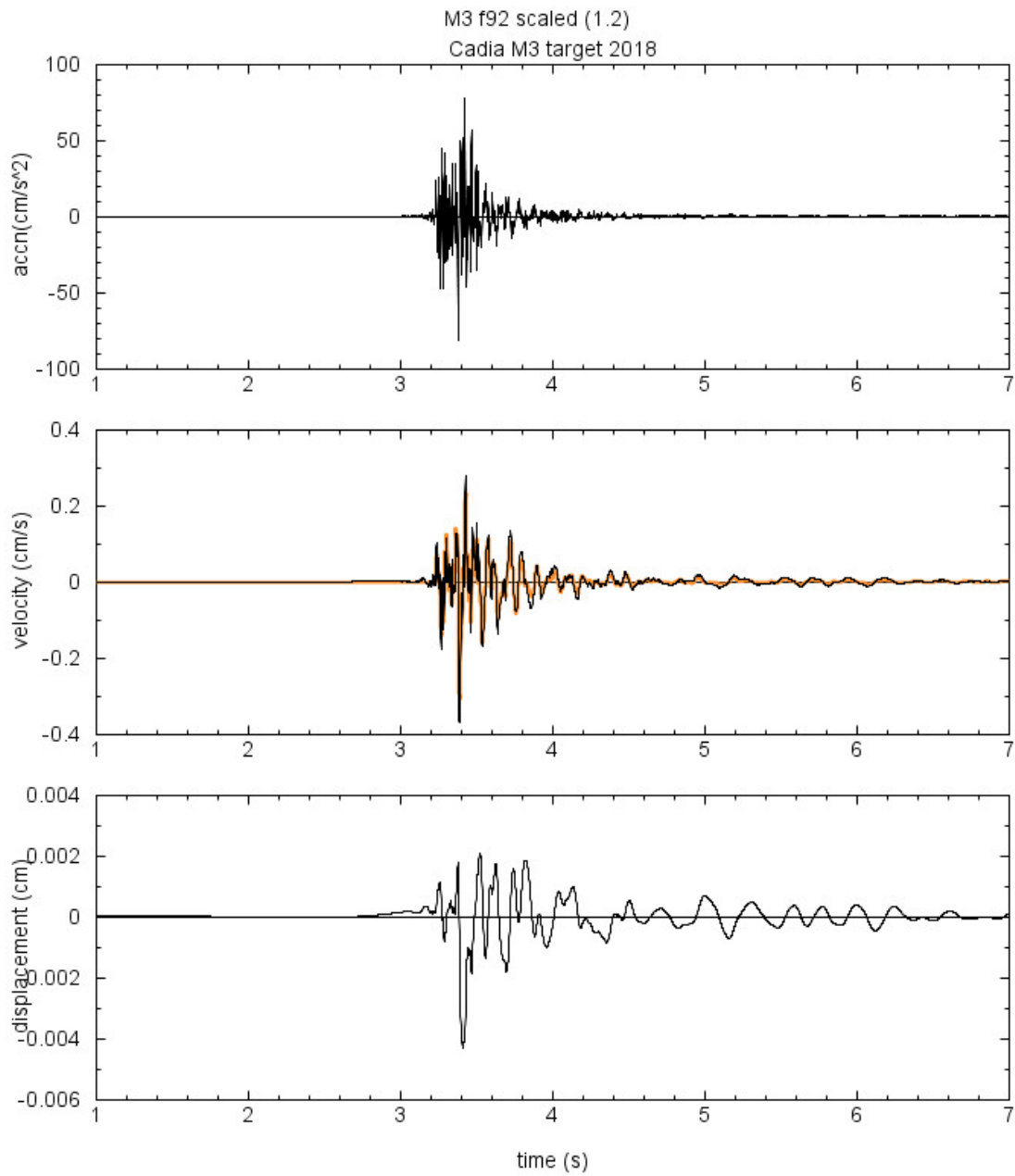
M3 f83 scaled (1.2)



M3 f90 scaled (1.2)



M3 f91 scaled (1.2)



M3 f92 scaled (1.2)

## **Appendix J:** **NTSF Project Document Referencing**

Reference Year	Reference Text
1995-001	Woodward-Clyde (1995). Cadia Project Tailings Disposal Study - Geotechnical Investigation Report. Document No. R002-A.
1995-002	Cadia Project Tailings Disposal – Phase II Feasibility Assessment, September 1995. Project No. 4541/2.2 Doc No. R001-A.D.
1997-001	Knight Piesold Pty Ltd (1997). Cadia Project - Tailings Storage Facility Design Report Volume 1. Ref. 217-6.
1997-002	Knight Piesold Pty Ltd (1997). Additional Site Investigation for Stage 1 of Cadia Tailings Dam. Report PSM231.R1.
1998-001	Knight Piesold Pty Ltd (1998). Cadia Tailings Storage Facility Stage 1 Embankment Construction Report.
1998-002	1998 Aerial Photograph.
2000-001	Woodward-Clyde (2000). Design Report Cadia Hill Tailings Storage Facility Stage 2A Augmentation.
2000-002	URS Australia Pty Ltd (2000). Cadia Hill TSF Stage 2A Construction Report.
2000-003	Woodward-Clyde (2000). Preliminary Geotechnical Report. Ridgeway Gold Mine Preliminary Investigation for Upper and Lower Rodds Creek Storage Facilities.
2000-004	Woodward-Clyde (2000). Cadia Hill Gold Mine Tailings Storage Facility Surveillance Report.
2002-001	URS Australia Pty Ltd (2002). Cadia Hill Gold Mine Northern TSF Stage 2B/1 Construction Report.
2003-001	URS Australia Pty Ltd (2003). Cadia Valley Operations Northern TSF Stage 2B/2 Construction Report.
2004-001	URS Pty Ltd (2004). Cadia Valley Operations Northern Tailings Storage Facility Stage 3 Design Report.
2006-001	URS Australia Pty Ltd (2006). Cadia Valley Operations Northern TSF Stage 3 Construction Report.
2006-002	2006 Aerial Photograph.
2007-001	URS Pty Ltd (2007). Cadia Valley Operations Northern Tailings Storage Facility, 2006 Surveillance Report.
2008-001	URS Australia Pty Ltd (2008). Cadia Valley Operations Northern TSF Stage 4 Construction Report.
2008-002	URS Pty Ltd (2008). Cadia Valley Operations Northern Tailings Storage Facility, 2008 Surveillance Report.
2009-001	URS Australia Pty Ltd (2009). Cadia Valley Operations Northern Tailings Storage Facility Stage 5 Design Report. Document Number 43167457.R010.
2010-001	2010 Aerial Photograph.
2010-002	URS Pty Ltd (2010). Cadia Valley Operations Northern Tailings Storage Facility, 2009 Surveillance Report.
2011-001	URS Australia Pty Ltd (2011). Cadia Valley Operations Northern TSF Stage 5 - Construction Report. Document Number 43167457.
2012-001	2012 Aerial Photograph.
2012-002	KCB (2012). Draft review report.
2013-001	URS Pty Ltd (2013). Cadia Valley Operations Northern TSF Stage 6 - Construction Report.
2013-002	URS Pty Ltd (2013). Cadia Valley Operations Northern Tailings Storage Facility Stage 7 Design Report.
2013-003	URS Pty Ltd (2013). Cadia Valley Operations Northern Tailings Storage Facility 2012 Surveillance Report.
2014-001	URS Pty Ltd (2014). Cadia NTSF Stage 7 Construction Report.
2014-002	URS Pty Ltd (2014). Cadia NTSF Stage 8 Design Report.
2014-003	URS Pty Ltd (2014). Cadia NTSF 2013 Surveillance Report.
2014-004	URS Pty Ltd (2014). Northern Tailings Storage Facility - Operation and Maintenance Manual.
2015-001	AECOM Services Pty Ltd (2015). Cadia Valley Operations Northern TSF Stage 8 Construction Report. Document Number R005.
2015-002	URS Pty Ltd (2015). Cadia NTSF Stage 9 Design Report.
2015-003	URS Pty Ltd (2015). Cadia NTSF 2014 Surveillance Report.
2016-001	Golder Associates (2016). Cadia Operations Tailings Laboratory Testing.
2016-002	AECOM (2016). Cadia North Tailings Storage Facility Interim Annual Surveillance Inspection May 2016.

Reference Year	Reference Text
2016-003	ATC Williams (2016). Cadia Valley Operations, NSW. North Tailings Storage Facility Surveillance Report 2016.
2016-004	GHD (2016). Newcrest Mining Cadia Tailings Dam Audit Report.
2017-001	ATC Williams (2017). Cadia Valley Operations Cadia, NSW. Northern Tailings Storage Facility Stage 10 Raise to RL 744 m Design Report. Report Number 115293.07R01 Rev 0.
2017-002	ATC Williams (2017). NTSF Foundation Investigation Test Pits. Reference Number 115293.07-M005.
2017-003	ATC Williams (2017). Cadia Valley Operations, NSW. Northern Tailings Storage Facility. Comprehensive Surveillance Report 2017. Document Number 115293.12 R04 Rev A DRAFT.
2017-004	ATC Williams (2017). KCB Peer Review of NTSF Stage 10 Design - Expanded ATCW Response.
2017-005	Klohn Crippen Berger (2017). Cadia TSF Peer Review - Site Visit.
2017-006	AECOM (2017). Cadia Valley Operations Northern TSF Stage 9 Construction Report.
2017-007	Golder Associates (2017). ATC Williams Stage 10 Raise Design Report - Comments.
2017-008	Stage 10 Construction Plan WE 2 Aug 2017.
2017-009	ATC Williams (2017). Stability memo
2017-010	ATC Williams (2017). Tailings investigation report.
2018-001	Photo sat 9-12-17 pic
2018-002	Photo sat 18-01-18 pic
2018-003	Photo sat 13-02-18 pic
2018-004	Photo sat 09-03-18 pic
2018-005	ATC Williams (2018). Cadia Valley Operations Cadia, NSW. Geotechnical Data Report. Northern and Southern Tailings Storage Facility Clay Foundation Geotechnical Investigation. Document Number 115293.15R02 Rev A.
2018-006	2018 NTSF prism monitoring raw data
2018-007	OTUS point data to 5 Sep 2018
2018-008	Cadia Valley Operations Independent Technical Review Panel (2018). Cadia North Tailings Storage Facility. Report 1.
2018-009	ATC Williams (2018). Site Visit Record - Inspection of the Northern Tailings Storage Facility at Cadia Valley Operations, near Orange, NSW. Document Number 115293.18 NTSF M013 Draft.
2018-010	Photograph of exposed foundation on 18th January 2018.
2018-011	Photograph of excavated face at toe of NTSF on 17th January 2018.
2018-012	Photograph of cracking on Stage 5 crest taken at 0748
2018-013	Photograph of Stage 8 crest cracking looking west
2018-014	Photograph of Stage 8 crest cracking looking east
2018-015	Photograph of cracking and heaving of haul road at Chainage 2060
2018-016	Larry Wright Incident Statement
2018-017	Peter Udy Incident Statement
2018-018	Steven Roberts Incident Statement
2018-019	Travis Small Incident Statement
2018-020	Peter Lord Incident Statement
2018-021	VWP Data File
2018-022	Spigot Opening Data
2018-023	10th March 2018 Orthophoto
2018-024	14th March 2018 Orthophoto
2018-025	Stage 1 Starter Embankment Sketch
2018-026	Stage 2A and 2B Embankments Sketch
2018-027	Stage 3 Embankment Sketch
2018-028	Stages 4 to 9 Embankment Sketch

---

Reference Year	Reference Text
2018-029	Stage 1 and 2 Buttress Construction Sketch
2018-030	NTSF West Drain Seepage Data
2018-031	OTUS point data to 25th Feb 2018
2018-032	OTUS image average velocity 1/17 to 2/18
2018-033	OTUS image average velocity 1/17 to 9/18
2019-01	<a href="https://youtu.be/IVD5H1YYnjU">https://youtu.be/IVD5H1YYnjU</a>
2019-02	<a href="https://www.youtube.com/watch?v=IVD5H1YYnjU&amp;feature=youtu.be">https://www.youtube.com/watch?v=IVD5H1YYnjU&amp;feature=youtu.be</a>
2019-03	GHD (2019) STSF Geotechnical Investigation and Stability Review - Geotechnical Investigation Report, Report for Cadia Holdings Pty Ltd